

“Babeş – Bolyai” University Cluj – Napoca
Faculty of Physics

Doctoral Thesis Summary

**STRUCTURAL INVESTIGATION ON SOME
MOLECULAR COMPLEXES OF BIOMEDICAL
INTEREST**

Ionuț – Bogdan Cozar

Scientific Supervisor,
Prof.dr. Leontin David

Cluj – Napoca

2011

CONTENTS

INTRODUCTION	2
1. Bases of some spectroscopic methods and of density functional theory (DFT)	3
2. IR, Raman, SERS and DFT studies on paroxetine	4
2.1. General data of paroxetine	4
2.2. Experimental and theoretical details.....	5
2.3. IR spectra analysis.....	6
2.4. Raman and SERS spectra	7
3. Vibrational and DFT studies of pindolol (PIN) and verapamil (VER) molecules	8
3.1. Characterization of PIN and VER molecules	8
3.2. IR spectra of PIN and VER	11
3.3. Raman and SERS spectra of PIN and VER	12
3.4. The adsorption of PIN and VER molecules on silver surface	14
4. Spectroscopic and DFT studies of atenolol (ATE) and metoprolol (MET) and their copper complexes	15
4.1. Characterization of ATE and MET molecules	15
4.2. IR and Raman spectra of ATE and MET	16
4.3. SERS spectra of ATE and MET	20
4.4. Cu(II) complexes of ATE and MET	21
5. Structural investigation of some metallic complexes with ligands of biomedical interest	24
5.1. Copper (II) complexes with ¹⁵ N – labeled amino acids	24
5.2. The identification of some monomeric species in the case of adsorption on NaY and HY zeolites	25
5.3. IR and NMR results on Pd(II) complex with theophylline and bipyridine	27
5.4. Structural informations obtained by X-ray diffraction and DFT calculations	28
Conclusions.....	30
References.....	32

KEY WORDS:

Pharmaceutical biomolecules, molecular spectroscopy, DFT calculations, ¹⁵N - isotope labeled amino acids, metal complexes

INTRODUCTION

Nowadays, there is an increasing emphasis on the life quality by improving the quality of drugs, medical investigation methods, diagnosis and treatment methods, with few secondary effects and totally elaborated.

In this context molecular spectroscopic studies (IR, Raman, SERS, NMR) for molecules of biomedical interest (drugs, amino acids, their complexes) are very important because of possible correlations between structure and molecular dynamics data provided by these methods and the physiological activity of the bio-molecules and related molecular systems.

The new structural data obtained this way lead to a deeper understanding of the physico-chemical processes occurring at the interaction of metal ions with ligand molecules, of the coordination place, the symmetry of local adopted structure, the action of various solvents and the induced biological effects or their stability at certain external factors.

Isotopic labeled amino acids, ¹⁵N-lysine and ¹⁵N-ornithine are used in a great variety of studies, as they are ideal internal standards for quantitative investigations of isotope labeled tracers in nutrition studies, to elucidate the details of the in vivo nitrogen metabolism and protein metabolism in various diseases.

In a similar way metal complexes of theophylline are of great importance in determining the interaction (coordination) mode of the metal ions with the biological purine derivatives - adenine and guanine, major components of DNA and RNA.

Due to an intense development in the last years of the information technology, both in terms of hardware and scientific software, quantum chemistry calculations and theoretical modeling by mean of density functional theory DFT at B3LYP/ 6-31G (d) level have a major contribution in the determination of the molecular structures, in the interpretation of experimental spectra and in the calculation of physico-chemical parameters that cannot be experimentally determined.

This information is used in the pharmaceutical industry to improve the therapeutic activity of drugs or to design and synthesize other new drug derivatives with special pharmaceutical properties.

1. Bases of some spectroscopic methods and density functional theory (DFT)

IR and Raman spectroscopies provide information about the vibration and vibration-rotation modes of molecules. Vibration-rotation bands are generally observed when the sample is in gaseous state, where the molecules are able to rotate freely. In the condensed matter, liquid or solid state, only vibration bands can be observed. IR and Raman spectroscopies are complementary techniques, some possible Raman transitions can be forbidden in IR or vice versa, depending on the symmetry of the molecule [1-3].

IR absorption and Raman scattering are optical spectroscopic methods that provide a high content of information regarding the molecular structure by identifying different vibration modes characteristic for bonds and atomic groups contained in the composition of the investigated molecules [4-7].

Particular attention is paid to SERS (Surface-Enhanced Raman Scattering) technique; it consists of a strong amplification of Raman signal if the molecules are adsorbed on the surface of nano-scale metallic structures [6-10]. Combining the structural information with ultra-sensitive Raman detection limits, SERS effect allows to elucidate the spatial orientation of the adsorbed molecules on different metal surfaces even at single-molecular level.

In the case of NMR spectroscopy, in addition to the basic principles, an emphasis is made on the “chemical shift”, its nature and the use of the obtained experimental data together with IR and Raman data to establish the coordination mode of metal ions with various molecules of biomedical interest [11-14].

At the end of the chapter the basic principles of DFT method are shown together with the basis sets of *Ab Initio* and DFT calculations, Slater and Gauss basis functions, minimal basis sets, split valence basis sets, extended basis sets, calculation of specific molecular properties of some given electronic states of IR and Raman spectra [13-16].

Special attention is also paid to the functional density theory (DFT) with B3LYP hybrid exchange-correlation functional and standard basis sets 6-31G(d) used to optimize molecular geometries, to calculate electrostatic molecular potential (MEP) and vibrational spectra.

2. IR, Raman, SERS and DFT study of paroxetine

2.1 General data on paroxetine

Structural investigations on compounds of biomedical and pharmacological interest are increasingly reported in the last years in the scientific literature. For this goal, experimental methods like FTIR, Raman, SERS, NMR and quantum chemical calculations based on density functional theory (DFT) were successfully used [17–18].

Thus, the structural characterization of paroxetine (3S,4R)-3-[(1,3-benzodioxol-5-yloxy)methyl]-4-(4-fluorophenyl)piperidine, a selective serotonin reuptake inhibitor antidepressant is welcome in this context. Paroxetine (Fig.2.1) is used to treat major depression, obsessive–compulsive, panic, social anxiety, and generalized anxiety disorders in adult outpatients [19].

The structures of (3R,4S)- and (3S,4R)-4-(4-fluorophenyl)- 3-hydroxymethyl-1-methylpiperidine compounds, which are intermediates in the synthesis of paroxetine and femoxetine pharmaceuticals, were studied previously by vibrational circular dichroism (VCD) spectroscopy [20].

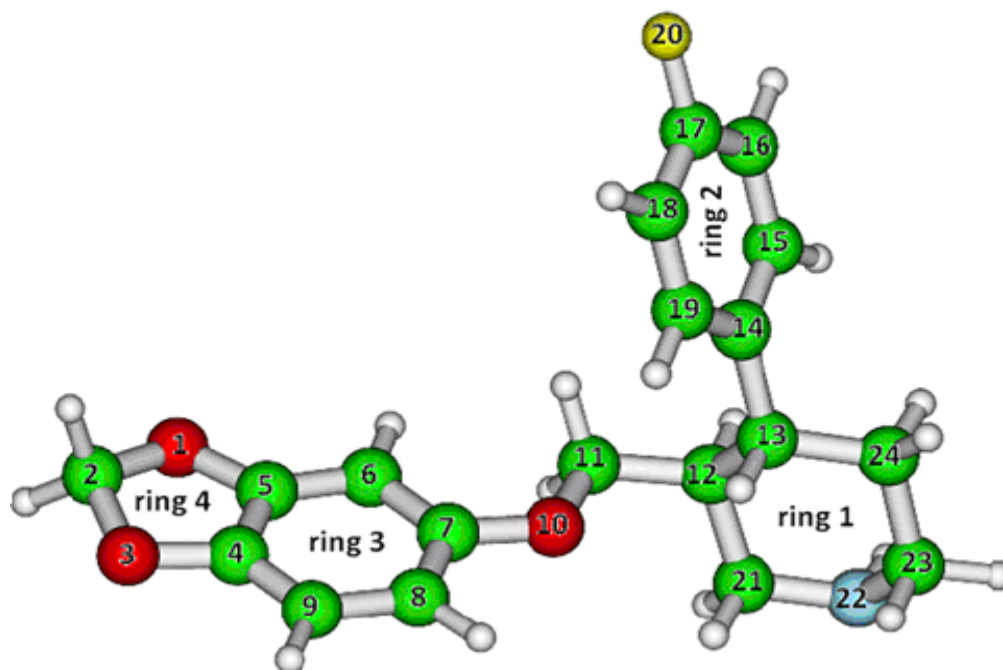


Fig.2.1. B3LYP/6-31G(d) optimized geometry of paroxetine with the atom and ring numbering scheme

X-ray structure of paroxetine hydrochloride salt has been reported [10–12] being shown that it exists in a non-hygroscopic hemihydrate form, thermodynamically the most stable, or a hygroscopic anhydrate form, the last one converting to form one when exposed to humid conditions or when compressed. β -Cyclodextrin inclusion complexes of paroxetine were produced as way of enhancing its chemical stability and solubility and have been quite recently investigated by Caira et al. [21].

The structural investigations by vibrational spectroscopic methods (FTIR, Raman and SERS), as well as density functional theory (DFT) based calculations performed on paroxetine molecule are reported in the paper [22]. To the best of our knowledge, assignment of the normal vibrational modes of paroxetine based on IR and Raman spectroscopies coupled with quantum chemical calculations has not been done so far.

2.2. Experimental and theoretical details

The FTIR spectrum of paroxetine powder sample was recorded at room temperature on a conventional Equinox 55 (Bruker, Germany) spectrometer equipped with a DTGS detector, coupled with an ATR sampling device (Miracle, Pike Techn.).

The FT-Raman spectrum was recorded with a resolution of 4 cm^{-1} in a backscattering geometry with a Bruker FRA 106/S Raman accessory equipped with a nitrogen cooled Ge detector. The 1064 nm Nd:YAG laser was used as excitation source, the laser power measured at the sample position was 300 mW.

The SERS spectrum was recorded using a DeltaNu Advantage spectrometer (DeltaNu, Laramie, WY) equipped with a doubled frequency Nd:YAG laser emitting at 532 nm. The laser power was 40 mW and the spectral resolution 10 cm^{-1} .

The silver colloidal SERS substrate was prepared by reducing Ag^+ with hydroxylamine [9]. The pH value of the silver colloid, measured immediately after preparation, was found to be 8.5.3.

Molecular geometry optimization, molecular electrostatic potential (MEP) and vibrational spectra calculations were performed with the Gaussian 03W software package by using density functional theory (DFT) methods with B3LYP hybrid exchange–correlation functional and the standard 6-31G(d) basis set [13]. No symmetry restriction was applied during geometry optimization. The vibrational frequencies were computed at the optimized

geometry to ensure that no imaginary frequencies were obtained confirming that it corresponds to a local minimum on the potential-energy surface.

2.3. IR spectra analysis

Experimental and calculated IR absorbance spectra of paroxetine in the 600–3500 cm^{-1} spectral range are shown in Fig. 2.2.

The most intense band in the IR spectrum is seen at 1183 cm^{-1} and it is excellently reproduced by quantum chemical calculation, both, in its position and intensity.

The bands situated at 765 cm^{-1} , 914 cm^{-1} and 931 cm^{-1} are due to bending vibrations of the piperidine ring and of C11H₂ group, respectively.

Bending vibrations of the ring3 are mainly contributing to the experimental bands at 781, 835, 944, 1097, 1183, 1247 and 1279 cm^{-1} , while normal modes corresponding to ring4 are associated with the experimental bands at 675 and 1381 cm^{-1} . Contributions from this ring are also seen in the normal modes assigned to the 781 and 944 cm^{-1} bands.

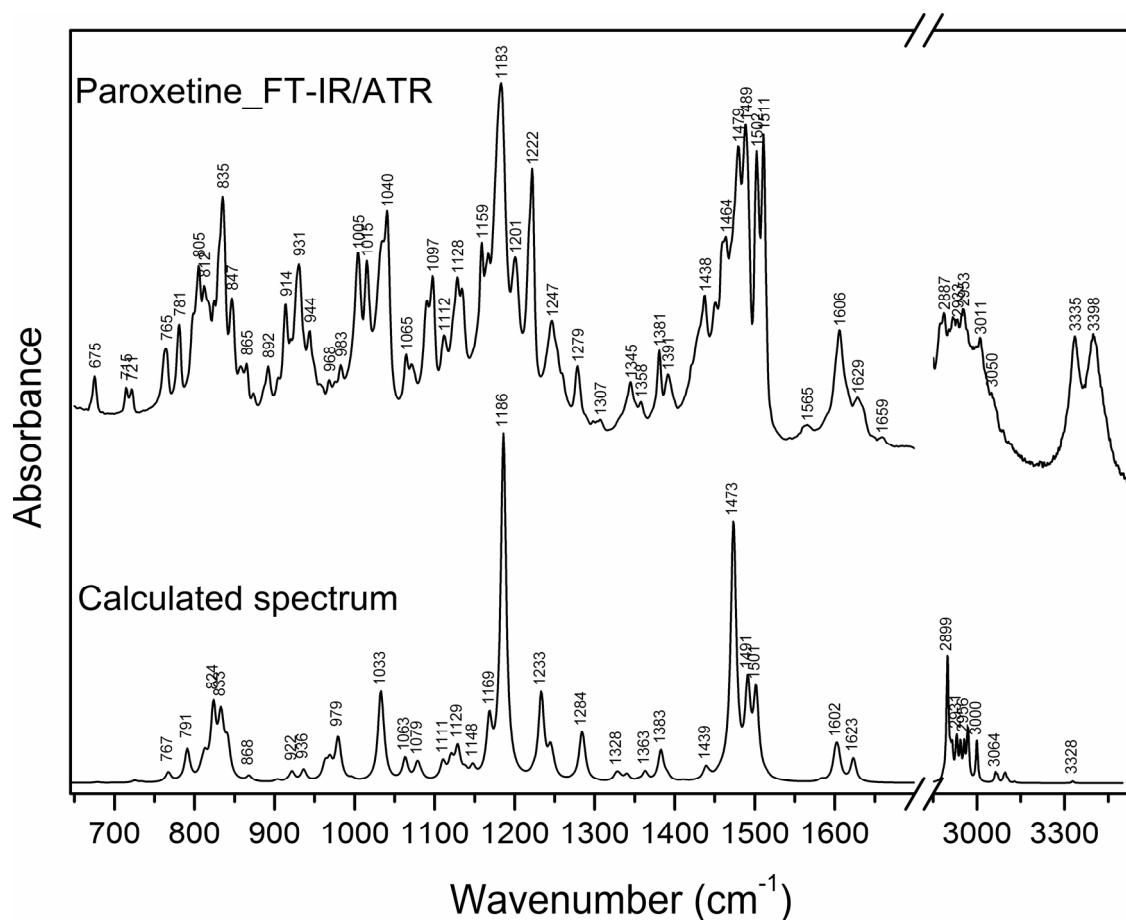


Fig.2.2. Experimental FTIR and calculated IR spectra of paroxetine

2.4. Raman and SERS spectra

Selected experimental SERS and FT-Raman bands, as well as their calculated wavenumbers and relative intensities at B3LYP/6-31G(d) level of theory are summarized in Table 2.1.

Significant changes can be observed in band positions and intensities by comparing Raman and SERS spectra of paroxetine, due to the interactions of the molecule with the silver nanoparticles surface. Thus, the most shifted SERS bands are those observed at 966, 1140, 333, 533, 582 and 1285 cm^{-1} . The SERS band at 966 cm^{-1} is blue-shifted by 20 cm^{-1} and corresponds mainly to CC stretching in ring1. It is also significantly enhanced giving thus evidence for a strong interaction of ring1 with the silver surface.

As it can be seen in the molecular electrostatic potential (MEP) map of paroxetine molecule (Fig.2.3.) obtained from DFT calculations, the negative charge is located mainly on the oxygen (O1, O3, O10) and piperidine nitrogen (N22) atoms.

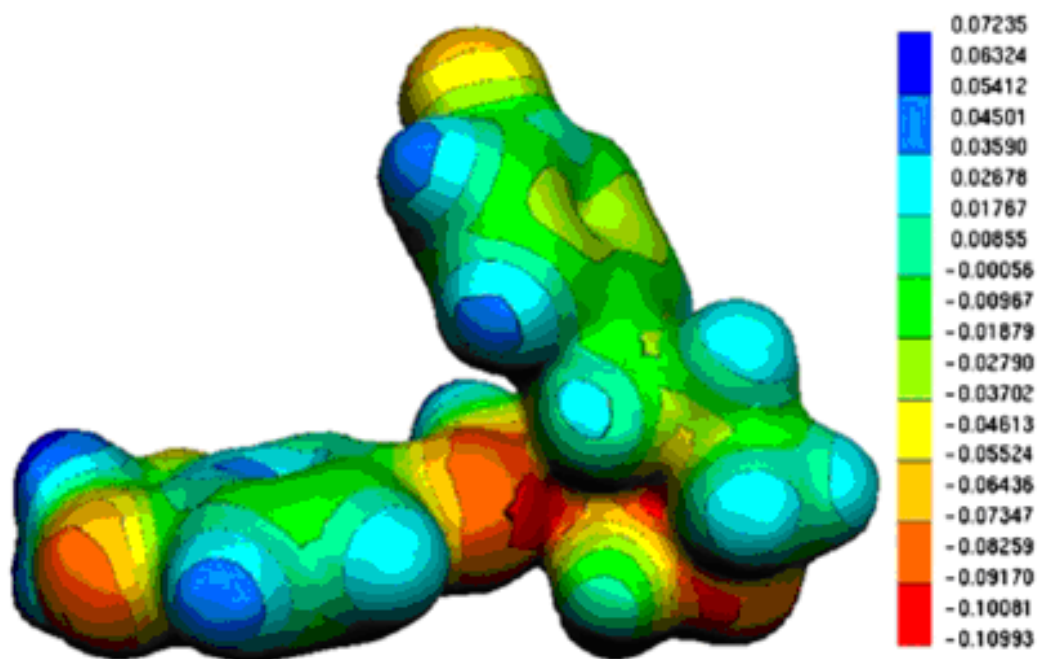


Fig.2.3. B3LYP/6-31G(d) calculated 3D electrostatic potential of paroxetine (a.u.) mapped onto the electronic density isosurface of 0.02 a.u.

Thus, when added to the silver colloidal solution, the adsorption of paroxetine to the nanoparticles surface is supposed to occur through the three oxygen and nitrogen atoms. This fact is illustrated by the appearance of an intense band at 243 cm^{-1} in the SERS spectrum,

characteristic for the vibration of Ag–O and Ag–N bonds, with no counterpart in the normal Raman spectrum. Similar values were reported for the wavenumbers assigned to Ag–N [23] or Ag–O [24] vibrations.

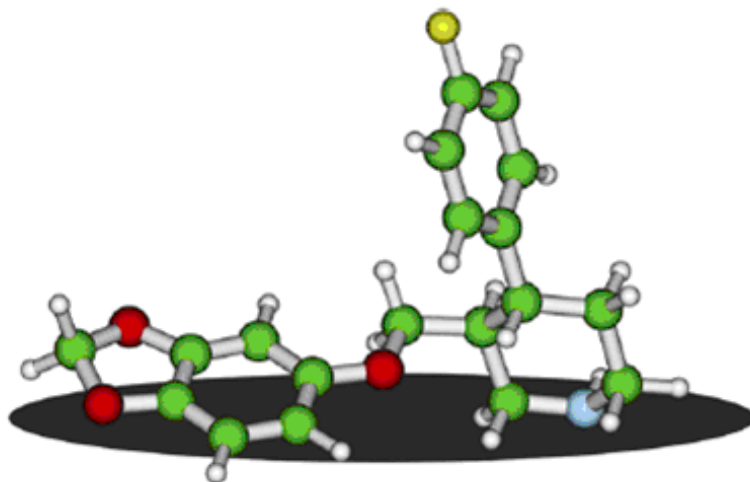


Fig.2.4. Suggested adsorption geometry of paroxetine molecule on the surface of silver nanoparticles

Table 2.1. Selected experimental SERS and FT-Raman bands, together with calculated wavenumbers and Raman intensities of paroxetine.

Experimental wavenumbers (cm ⁻¹)				Calculated wavenumbers cm ⁻¹		Band assignment
SERS	I _S	FT-Raman	I _R	B3LYP	I	
1605	41	1604	99	1603	50	v(CC ring3)+δ(CH ring3)
1504	11	1502	39	1514	33	δ(C2H ₂)
1452	26	1468	51	1444	37	δ(CH ₂ , CH, NH)
1363	47	1358	66	1355	18	δ(CH ₂ , CH ring1)+δ(C11H ₂)
1288	20	1297	39	1285	40	v(CC ring3)+δ(CH, CH ₂ ring1)
1223	41	1218	92	1234	52	δ(CCC ring2)+τ(CH ₂)
1198	31	1197	53	1178	45	v(C13C14)+δ(CH ring2)+δ(C13H)
1140	71	1159	42	1168	22	τ(C2H ₂)+v(C7O10)
1090	13	1094	27	1079	16	δ(OCC ring4)+δ(ring3, ring4)+ v(C11C12)
1062	26	1063	21	1063	18	v(CO ring4)+δ(CCC ring3)+v(C11C7)
988	42	982	24	979	25	δ(CCC ring1)+v(O2C11)
966	37	946	13	969	30	v(CC ring1)+δ(CH, CH ₂ , NH ring1)
844	47	846	56	868	51	breathing(ring2)+δ(CH, CH ₂ , NH ring1)
812	67	805	100	835	100	breathing(ring3+ ring4)+δ(CH ring3)
715	22	720	35	734	54	v(CO ring4)+v(CC ring3)+δ(C2H ₂)
676	14	675	6	678	10	δ(ring1,3,4)+δ(O10C11C12)
631	28	635	35	650	39	v(CC ring2)+δ(CH ring2)
584	17	573	21	583	24	δ(ring1, ring2, ring3)
535	19	522	11	524	18	δ(CCC ring1,2,3)+δ(C7O10C11)
478	18	470	11	476	18	δ(ring1)
347	19	351	35	343	91	γ(ring3, ring 4)+ρ(C11H ₂)
		253	26	252	99	δ(ring1, ring2)
243	100					v(AgO)+v(AgN)

I_S-SERS intensity, I_R-Raman Intensity; I-Intensity, v- stretch, v_s- symmetric stretch, v_{as}- asymmetric stretch, δ- in plane bending, ρ-rocking, τ-twisting, ω-wagging, γ-out of plane bending, ring1: piperidine ring (N22-C21-C12-C13-C24-C23); ring2: fluorophenyl ring (C14-C15-C16-C17-C18-C19); ring3: benzene ring (C4-C5-C6-C7-C8-C9); ring4: dioxolane ring (O1-C2-O3-C5-C4)

Moreover, in order to simulate the interaction of the molecule with the silver surface we optimized two complexes formed between paroxetine molecule and one Ag atom arranged in the vicinity of the N22 atom of the molecule or in the close vicinity of dioxolane ring (O). B3LYP functional was used with 6-31G(d) basis set for the atoms of the molecule and Lanl2dZ effective core potential and basis set for Ag atom. Our calculated wavenumbers are 244 cm^{-1} for Ag–N vibration and 226 cm^{-1} for Ag–O vibration. In consequence the 243 cm^{-1} band comes from Ag-N22 interaction.

Based on the analysis of SERS and Raman spectra and considering the MEP map of this molecule and the SERS selection rules, the adsorption mode of paroxetine to silver nanoparticles was shown to occur through the oxygen and nitrogen atoms.

The benzodioxol ring is adsorbed in a tilted orientation, in the near vicinity of the silver surface, while the piperidine ring and benzene ring are perpendicular oriented on the silver surface.

3. Vibrational and DFT studies of Pindolol and Verapamil

3.1. Characterization of PIN and VER molecules

The structural investigation of pindolol (PIN) and verapamil (VER) molecules (Fig.3.1) is welcome because of their large implications in medicine. Thus, pindolol is a nonselective beta blocker with partial beta-adrenergic receptor agonist activity. In high doses it increases pulse rate, blood pressure and bronchodilation showing also membrane stabilizing and antiarrhythmic effects [25]. Verapamil is an L-type calcium channel blocker of the phenylalkylamine class. It has been used in the treatment of hypertension, angina pectoris, cardiac arrhythmia, and most recently, cluster headaches. It is also an effective preventive medication for migraine and more effective than digoxin in controlling ventricular rate [26].

Many important results on the pindolol structure obtained by infrared spectroscopy and natural bond orbital (NBO) theory and also on the mechanism of the ring contraction of oxazinones to oxazolidinones are given in the papers [27]. Thus, Castro et al. [27] have identified the characteristic absorption vibrational bands of the spectra of solid pindolol and of the isolated conformer and performed the structure optimization at the DFT level of theory using the B3LYP functional and the 6-31G* basis set.

Previous experimental and theoretical works have been also reported on the polymorphism and gas-phase conformers of this compound [28].

The most stable conformation of verapamil was determined theoretically by Fernandez et al. [29] using the molecular mechanics approaches and the greater conformational stability was related to the coplanar arrangement of the phenyl and cyano groups.

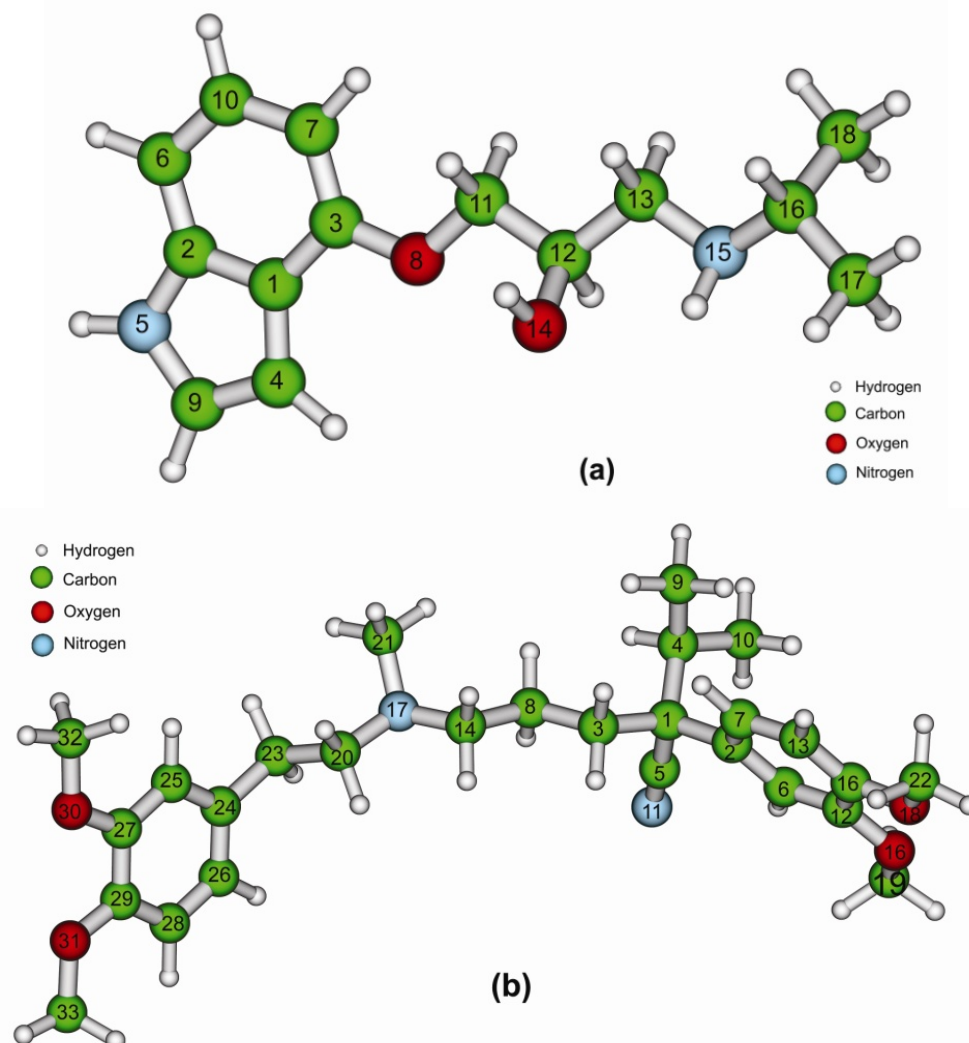


Fig.3.1. B3LYP/6-31G(d) optimized molecular structures of pindolol (a) and verapamil (b)

In this study, the IR, Raman and SERS spectra of PIN and VER molecules correlated with their structural aspects are discussed [30]. The assignment of the vibrational bands is accomplished by DFT calculations.

It is worth mentioning here that the experimental geometry of pindolol, reported by Chattopadhyay et al. [31] is stabilized by two intra-molecular $\text{NH} \cdots \text{O}$ and $\text{OH} \cdots \text{O}$ hydrogen bonds and consequently, the vibrations associated with these groups are expected to be influenced by the hydrogen bonding interactions.

Moreover, Nunes and colleagues [28] have shown that different polymorphic forms of this compound exist and that commercial pindolol presents two of these forms.

As starting geometry for the optimizations process, for both compounds we used the structures found in the DrugBank database [32]. Also, our optimized bent configuration of verapamil, with an almost coplanar arrangement of the cyano and phenyl groups is analogue with that given in the paper [29].

3.2. IR spectra of PIN and VER

The B3LYP/6-31G(d) optimized geometry of pindolol is given in Fig.3.1. Excepting very few geometrical parameters, it is in a surprisingly good agreement with the experimental one [31]. Moreover, a very similar conformer (E_2 denoted TTTTGT') was identified by Nunes et al. [33], being defined by $\varphi_1 = 180.0^\circ$, $\varphi_2 = -177.0^\circ$, $\varphi_3 = 179.0^\circ$, $\varphi_4 = 177.0^\circ$ and $\varphi_5 = 172.0^\circ$. Our corresponding calculated dihedrals (-178.7° , 178.8° , 175.3° , -177.3° and -166.8°) compare very well with those reported in [33], being also in qualitative and quantitative agreement with the experimental counterparts (177.2° , 162.2° , 176.9° , -178.0° and -162.6°) [31].

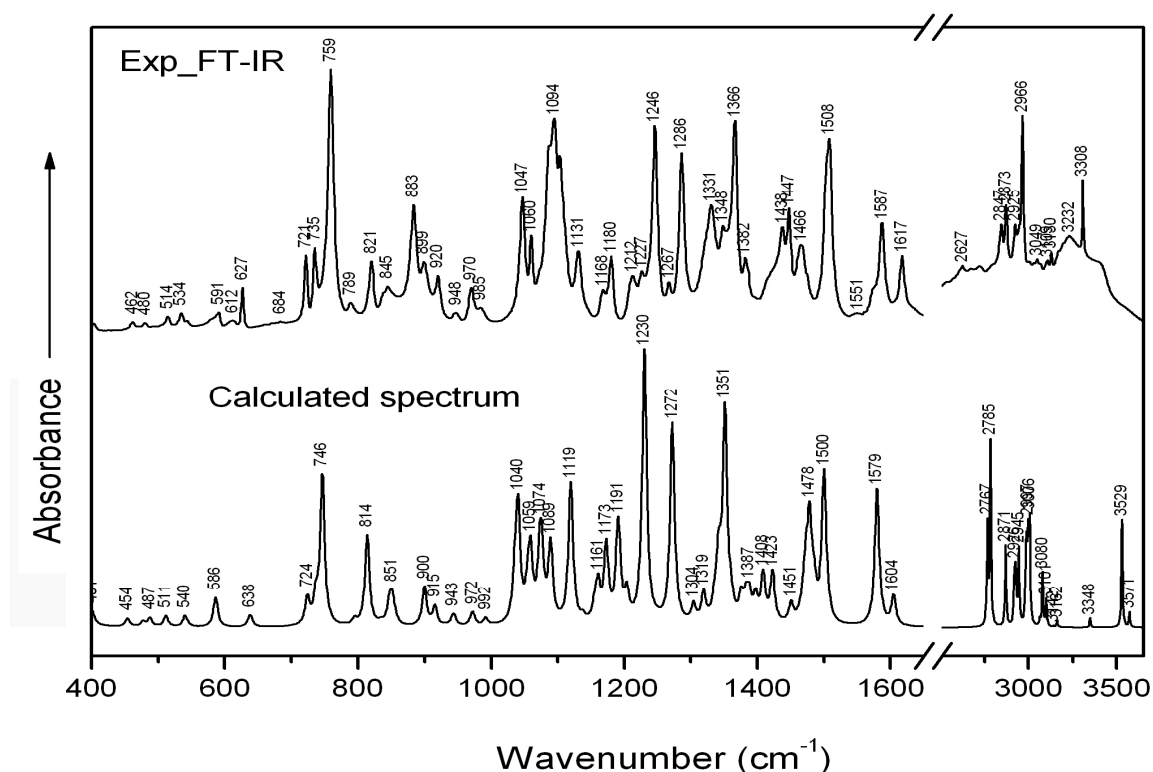


Fig.3.2. Experimental FT-IR and calculated IR spectra of PIN

As it can be seen from Fig. 3.2 and data summarized in Table 3.1, a number of bands can be considered as being representative for pindolol. The minor differences between our

assignments given in Table 3.1 and those provided by Castro et al. [27] are, most probably due to small differences in the two optimized geometries.

Thus, the band at 759 cm^{-1} is due to the out of plane bending vibration characteristic of O14H group. The band from 883 cm^{-1} is due to the superposition of the out of plane deformation vibrations of N15H group with the in plane deformations of aliphatic carbon (C11C12C13) chain. The stretching vibration of C11O8 group and in plane bending vibration of CH groups appear at 1047 cm^{-1} .

Table 3.1. Selected experimental FT-IR bands and B3LYP/6-31G(d) calculated wavenumbers of PIN (cm^{-1})

Experimental FT-IR	Calculated wavenumber*	Assignments
591	586	ip. ring1 deformation+ $\delta(\text{CH}_2)$ + $\delta(\text{CH})$
627	638	ip. ring1, ring2 deformation+ $\delta(\text{CH}_2)$ + $\delta(\text{CH})$
721	724	$\gamma(\text{C-H})$ indole i.p.
759	746	$\gamma(\text{O14H})$
821	814	$\delta(\text{NH})$ + $\rho(\text{CH}_3)$
883	900	$\gamma(\text{N15H})$ + $\delta(\text{C11C12C13})$
1047	1040	$\nu(\text{C11-O8})$ + $\delta(\text{CH})$
1060	1059	$\delta(\text{C2N5C9})$
1094	1089	$\rho(\text{C11-H2})$, $\nu(\text{C14-N15})$ i.p.+ $\gamma(\text{C12-OH})$
1131	1119	$\delta(\text{N5-H})$, $\delta(\text{C-H})$ indole o.p.
1180	1190	$\rho(\text{CH}_2)$ + $\delta(\text{NH})$ + $\delta(\text{CH})$
1246	1230	$\delta(\text{N5-H})$, $\delta(\text{C7-H})$, $\delta(\text{C10-H})$, $\delta(\text{C6-H})$ i.p.
1286	1272	$\delta(\text{C5-O10})$ + $\delta(\text{CH})$ + $\delta(\text{NH})$
1366	1351	$\delta(\text{CCC ring1})$ + $\delta(\text{CNC ring2})$ + $\delta(\text{CH})$ + $\delta(\text{NH})$
1466	1478	$\delta(\text{CH}_2)$ + $\delta(\text{CH}_3)$ + $\delta(\text{N15H})$
1508	1500	$\delta(\text{N5-H})$ + $\delta(\text{C11H}_2)$
1587	1579	$\nu(\text{C1=C2})$, $\nu(\text{C7=C10})$
1617	1604	$\nu(\text{C1=C3})$, $\nu(\text{C6=C2})$
2873	2871	$\nu_s(\text{C13H}_2)$
2966	2945	$\nu(\text{C-H})$ aliphatic
3308	3348	$\nu(\text{N15-H})$

ν - stretch, ν_s - symmetric stretch, ν_{as} - asymmetric stretch, δ - in plane bending, ρ - rocking, γ -out-of-plane bending, def.-deformation, ip.-in plane, op.-out of plane

*-scaled values according to Scott and Radom [34]; ring1: benzene ring(C2-C1-C3-C7-C10-C6); ring2: pyrroline ring (C1-C2-N5-C9-C4)

The superposition of the in plane vibrations of the ring NH and CH groups, and also of C5A010 group with NH, CH groups, are situated at 1246 cm^{-1} and 1286 cm^{-1} respectively. The in plane deformations of CCC and CNC groups from benzene and pyrroline rings are superposed at 1366 cm^{-1} .

Another intense superposition of in plane bending vibrations of N5H and C11H2 groups appear at 1508 cm^{-1} . At high wavenumbers 2873, 2966 and 3308 cm^{-1} the stretching vibrations of C13H₂, CH aliphatic and N15H groups appear, too.

3.3. Raman and SERS spectra of PIN and VER

Raman, SERS and calculated spectra of verapamil are shown in Fig. 3.3. Selected experimental SERS, FT-Raman bands and calculated corresponding to the most intense Raman intensities are given in Table 3.2.

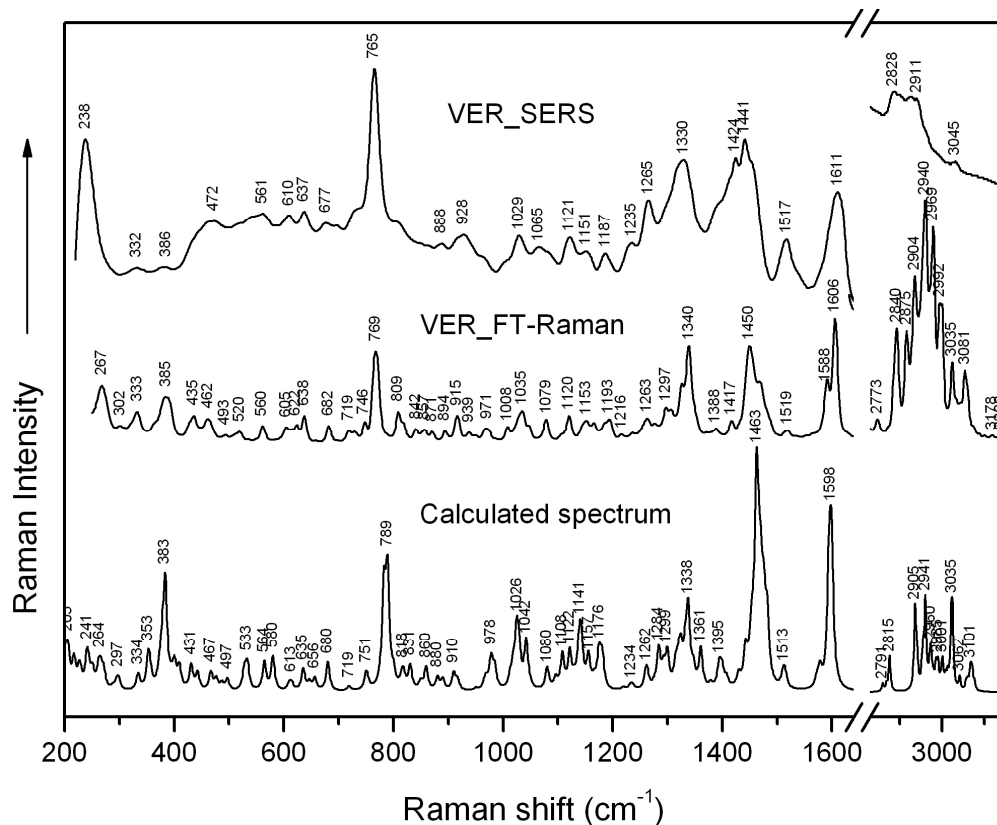


Fig.3.3. SERS, FT-Raman and calculated Raman spectra of VER

Table 3.2. Selected experimental SERS, FT-Raman bands and B3LYP/6-31G(d) calculated wavenumbers of VER (cm^{-1})

Experimental		Calculated	
SERS	FT-Raman	wavenumber*	Assignments
238			
	267	264	$\rho(\text{CH}_3)$
378	385	383	$\delta(\text{O31CH}_3, \text{O30CH}_3, \text{O16CH}_3, \text{O18CH}_3, \text{CH}_3)$
765	769	789	$\nu(\text{CC ring1}) + \text{ip. ring1 deformation} + \delta(\text{CH ring1}) + \delta(\text{CH}_3) + \nu(\text{C12O16}, \text{C15O18})$
1029	1035	1026	$\nu(\text{CC ring1}) + \nu(\text{O16CH}_3, \text{O18CH}_3)$
1330	1340	1338	$\delta(\text{CH}_2) + \rho(\text{CH}_2) + \nu(\text{CC ring1})$
1441	1450	1463	$\delta(\text{CH}_3) + \delta(\text{CH}_2)$
1517	1519	1513	$\nu(\text{CC ring1}) + \delta(\text{CH ring1}) + \nu(\text{C12O}, \text{C15O})$
1611	1606	1598	$\delta(\text{O16CH}_3, \text{O18CH}_3) + \delta(\text{CH}_3)$
2826	2840	2815	$\nu(\text{C20H54}, \text{C14H49}, \text{C21H56})$
2911	2940	2941	$\nu_s(\text{C10H}_3, \text{C9H}_3, \text{C3H}_2, \text{C8H}_2)$
3045	3035	3035	$\nu_{as}(\text{C32H}_3, \text{C33H}_3)$

ν - stretch, ν_s - symmetric stretch, ν_{as} - asymmetric stretch, δ - in plane bending, ρ - rocking, γ -out-of-plane bending, def.-deformation, ip.-in plane, op.-out of plane.

ring1: benzene ring(C2-C6-C12-C15-C13-C7); ring2: benzene ring(C24-C29).

*-scaled values according to Scott and Radom [34].

Significant changes can be observed in band positions and intensities by comparing the Raman and SERS spectra of VER, due to the interaction of VER molecule with the silver surface.

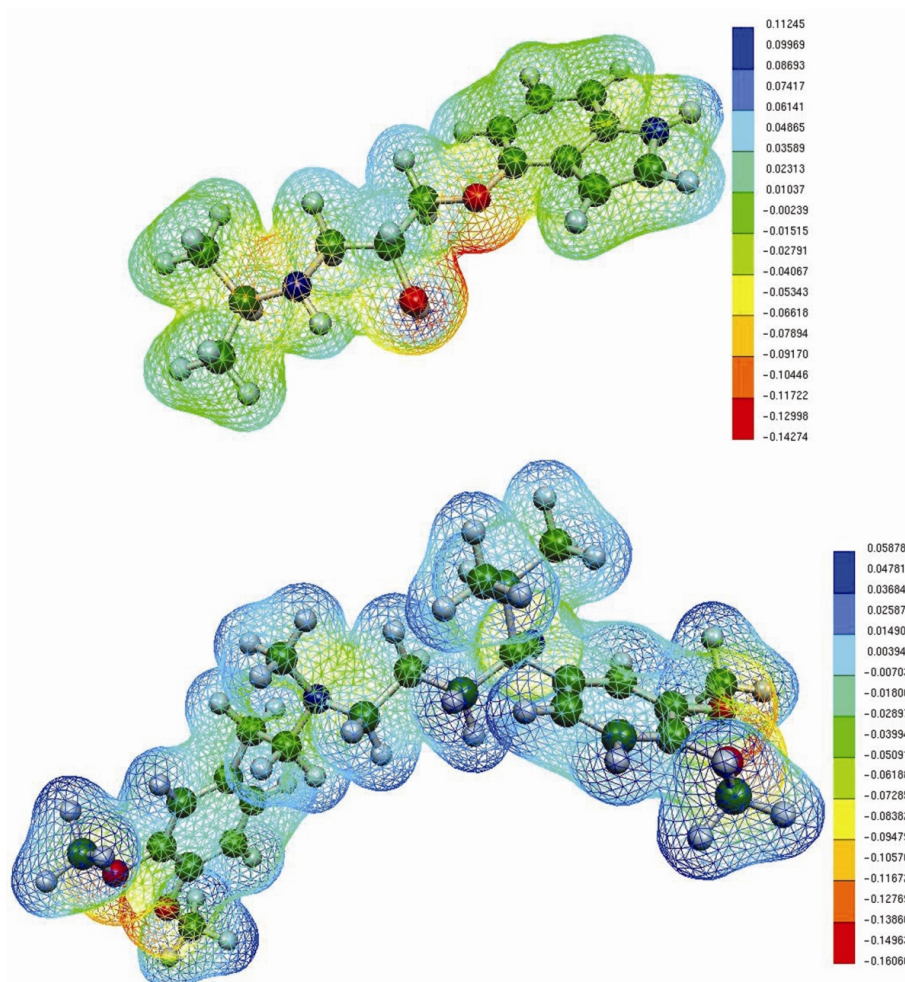


Fig. 3.4. B3LYP/6-31G(d) calculated 3D electrostatic potential contour map of PIN (top) and VER (bottom) in atomic units

3.4. The adsorption of PIN and VER molecules on silver surface

As it can be seen in the MEP distribution of the PIN molecule (Fig. 3.4.) obtained from DFT calculations, the negative charge is located mainly on the oxygen atoms (O8, O14) and the nitrogen atoms (N15 from aliphatic chain and N5 from pyrrolidine ring). Thus, when added to the silver colloidal solution, the adsorption of the molecule to the silver surface is supposed to occur through the oxygen (O8, O14) atoms.

This fact is illustrated by the 240 cm^{-1} band which appears in the PIN SERS spectrum, characteristic for the Ag-O bond. However, an adsorption through the π -electrons, of the aromatic rings is also plausible, as shown by the MEP distribution and by charge of the two nitrogen atoms (N5, N15).

We can thus finally conclude that the whole structure of PIN lies on the silver surface in a flat orientation [35].

The bands $769, 1035, 1340, 1450, 1519\text{ cm}^{-1}$ from Raman spectrum, due to the stretching C-C rings (1 and 2) vibrations and deformation vibrations of CH_2, CH_3 groups, increase in intensity in the SERS spectrum and are shifted to lower wavenumbers (Table 3.2.).

An intense band at 238 cm^{-1} due to the Ag-O bond formation appears also in the SERS spectrum of VER due to a strong interaction of its oxygen atoms (O16, O18 and O30, O31), bonded to the benzene rings, with the silver nanoparticles surface.

Taking into account the SERS surface selection rules [6,7] and the MEP of VER (Fig. 3.4.) which shows that the negative charge is located mainly on the four oxygen atoms (16, 18, 30, 31) we can finally conclude that the VER molecule adopts a bent conformation on the silver surface, strongly fixed by the oxygen atoms and a perpendicular orientation of the benzene rings to the silver surface.

4. Spectroscopic and DFT study of atenolol and metoprolol and their copper (II) complexes

4.1. Characterization of ATE and MET molecules

Atenolol (4-[20-hydroxy-30-[(1-methylthyl)amino]propoxy]-benzeneacetamide – ATE) and metoprolol (1-(isopropylamino)-3-[p-(2-methoxyethyl)phenoxy]-2-propanol – MET), shown in Fig.4.1, are widely prescribed in medicine as cardioselective β_1 -adrenergic blockers [36, 37].

Since different conformations or enantiomers of such molecules can drastically influence their physico-chemical behavior and pharmacological activity, the knowledge of their structures is of most importance.

In this study, IR, Raman and SERS spectra of ATE and MET, as well as IR and EPR spectra of their copper complexes are discussed. The assignment of the vibrational bands is accomplished by DFT calculations at B3LYP/6-31G(d) level of theory.

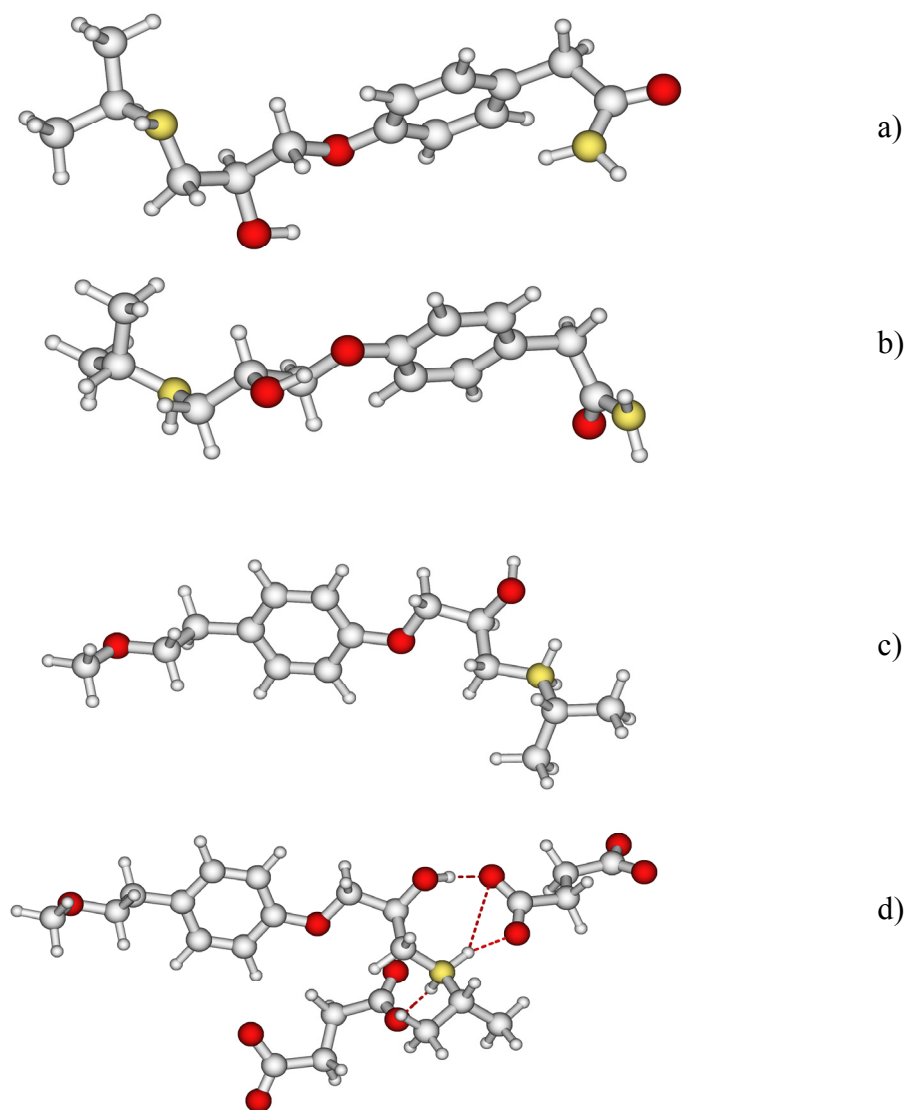


Fig. 4.1. B3LYP/6-31G(d) optimized geometries of (S)-atenolol (a) and (R,S)-atenolol (b), metoprolol (c) and the complex metoprolol-2 succinate anions (d)

Previously reported studies on vibrational properties of ATE are focused particularly on hydrogen bonding interactions [36] and the interaction between ATE and β -cyclodextrins.

On the other hand, to the best of our knowledge, no detailed vibrational analysis was reported so far for metoprolol. X-ray structure of this compound was reported recently [38] being shown that MET crystallizes in an N-protonated form, being hydrogen bonded to two succinate anions.

4.2. IR and Raman spectra of atenolol and metoprolol

Vibrational spectra of both molecules were calculated by using optimized geometries at B3LYP/6-31G(d) level of theory.

The two conformers (R,S)- and (S)- ATE differ in the relative orientation of both, acetamide and methyl-ethyl-amino-propoxy side chains (Fig. 4.1.). Even though quite large differences are noted between the dihedral angles defined by the same atoms in the two conformers of ATE, the energetic difference between conformers is as low as 1.14 kcal/ mol, the (S) conformer being the most stable.

For MET we optimized the protonated and unprotonated forms, as well as the molecular complex formed between the N-protonated MET cation and two hydrogen bonded succinate anions using as starting geometries the experimental structures [38].

The main difference between the HB and non-HB MET is a slightly different orientation of the two terminal CH₃ group relative to the neighbor amino group, as well as a change in the lengths of the H₂C–NH₂ and H₂N–CH bonds. Thus, in the non-HB conformer, the two bond lengths are 1.510 and 1.531 Å, while for the MET-2 succinate complex they are significantly shorter (1.494 and 1.508 Å).

Some experimental results together with the calculated wavenumbers and normal modes assignments suggested by DFT calculations are given in Table 4.1. and Fig. 4.2.

Overall, the calculated IR and Raman spectra of the (S)- and (R,S)-ATE conformers are similar, both, in band positions and their intensities. As seen in Table 4.1, the Q4, Q8, Q9, Q12, Q14 and Q21 modes are predicted almost equally well by both (S) and (R,S) conformers.

However, some differences are noted either between the calculated wavenumbers and activities of the two conformers or between the experimental and calculated intensities; such modes are: Q11, Q13, Q15, Q17, Q18, Q22, Q24-Q26 and Q28.

The Q11, Q18 and Q25 modes are predicted only by the (S) conformer, while for Q13, Q15, Q24, Q26 and Q28 the same conformer predicts better band positions and/or intensities when compared to the (R,S) conformer. As shown in Table 4.1., both conformers predict Q17 mode too high in energy and much weaker than seen in the experimental spectrum, while the Q22 mode is predicted well in its position but, again, much weaker than its experimental counterpart.

Based on this analysis we conclude that (S) enantiomer is mainly responsible for the appearance of IR and Raman spectra of ATE, even though contributions from the (R,S) conformer are present.

This is in perfect agreement with Ruperez and Laserna [39] who have shown in addition that the racemic and (S) forms of ATE can be differentiated based on the two Raman bands at 1609 and 1038 cm⁻¹, the second band being characteristic for the racemic mixture.

Table 4.1. Experimental and B3LYP/6-31G(d) calculated vibrational spectra of atenolol [cm⁻¹]

Mode	Experimental		Calculated*				Assignments
	FT- IR/ATR	Raman	(S)-ATE		(RS)-ATE		
			IR	Raman	IR	Raman	
Q1			3588 vw		3586 vw	3586 w	$\nu(\text{OH})$
Q2	3356 s		3574 w	3574 vw	3554 vw	3554 w	$\nu_a(\text{NH}_2)$
Q3	3174 m		3453 vw	3453 m	3437 vw	3437 m	$\nu_s(\text{NH}_2)$
Q4		3070 s		3089 m	3052 vw	3087 s	$\nu(\text{CH ring})$
Q5	2965 w	2969 s	2990 w		3007 vw	3007 s	$\nu_a(\text{CH}_3)$
Q6	2924 w	2915 vs		2923 vs	2952 vw	2933vs	$\nu_s(\text{CH}_3)$
Q7	1670 sh	1681 w					$\nu(\text{CO})$
Q8	1637 vs		1736 vs	1736 vw	1736 vs	1736 vw	$\nu(\text{CO})$
Q9	1612 w	1612 s	1607 w	1608 s	1607 w	1607 s	$\nu(\text{CC ring})$
Q10			1571 s	1570 s	1587 s		$\delta(\text{NH}_2)$
Q11	1583 vw	1583 w	1567 vw	1567 vw			$\nu(\text{CC ring})$
Q12	1517 m		1504 m		1503 m		$\nu(\text{CC ring})+\delta(\text{CH ring})+\delta(\text{CH}_2)$
Q13		1450 m		1449 w	1475 w	1461 w	$\delta(\text{CH}_3)$
Q14	1418 w	1421 w	1408 vw		1407 vw		$\delta(\text{COH})+\omega(\text{CH}_2)$
Q15	1302 vw	1301 m	1310 w	1312 vw	1334 m		$\delta(\text{OCNH}_2)+\delta(\text{CCC ring})$
Q16	1243 m	1243 w	1245 s	1277 w	1244 vs	1267 vw	$\omega(\text{CH}_2)$
Q17		1205 s	1229 m	1228 vw	1226 m	1226 vw	$\delta(\text{CH})+\delta(\text{OH})+\delta(\text{CCC ring})$
Q18	1180 vw	1183 m		1186 vw			$\nu(\text{CC})+\delta(\text{CCC ring})+\omega(\text{CH}_2)$
Q19		1141 m	1158 w	1166 vw	1135 vw	1149 vw	$\nu(\text{HC-NH})+\rho(\text{CH}_3)$
Q20	1038 vw	1038vw	1025 w		1030 w		$\nu(\text{C-O})+\rho(\text{CH}_3)+\delta(\text{CH ring})$
Q21	886 vw	886 m	888 vw	887 vw		888 w	ring breathing
Q22		859 vs		869 vw		865 vw	$\delta(\text{CCC ring})$
Q23	829 vw	829 m		826 vw	817 vw	836 vw	$\delta(\text{CCC ring})+\rho(\text{NH}_2)$
Q24	712 vw	722 m	749 vw	749 vw	759 vw	759 vw	$\delta(\text{NH})$
Q25		638 m		653 vw			$\delta(\text{CCC ring})+\tau(\text{NH}_2)$
Q26	568 vw	568 vw	558 vw		597 w		$\tau(\text{ring})+\delta(\text{OC-NH}_2)$
Q27	427 vw		429 vw		430 vw		$\delta(\text{OH})$
Q28		368 vs	256 vs	362 vw	372 vs	345 vw	$\omega(\text{NH}_2)$

vs – very strong, s – strong, m – medium, w – weak, vw – very weak, sh – shoulder.

* scaled wavenumbers according to the procedure proposed by Scott and Radom [34]

Vibrational spectra of MET are given in Fig. 4.2. By comparing the experimental and calculated wavenumbers for N-protonated MET (MET⁺) and for MET⁺-2 succinate anions complex (MET⁺-2 SA²⁻) the following conclusions result.

The major difference between the spectra given by the two structures is seen in the high wavenumber region. Thus, the Q1– Q3 modes of MET⁺-2 SA²⁻ are, as expected, reproduced at significantly lower wavenumbers than in the case of non-H bonded MET⁺. Particularly, the two bands at 2451 and 2550 cm⁻¹ in the experimental IR spectrum are qualitatively and almost quantitatively reproduced by the H-bonded complex.

On the other hand, for the same complex, the predicted the red shift of $\nu(\text{OH})$ band seems to be much too pronounced. An explanation for this behavior can be given considering the difference between the calculated and experimental OH...O intermolecular distance for this HB complex.

The calculated value (2.667 Å) is significantly lower than that given by experiment (2.723 Å). The same behavior is observed for the lengths of the two NH bonds in the amino group whose experimental values are 2.745 Å and 2.796 Å, while their calculated values are 2.692 Å and 2.708 Å.

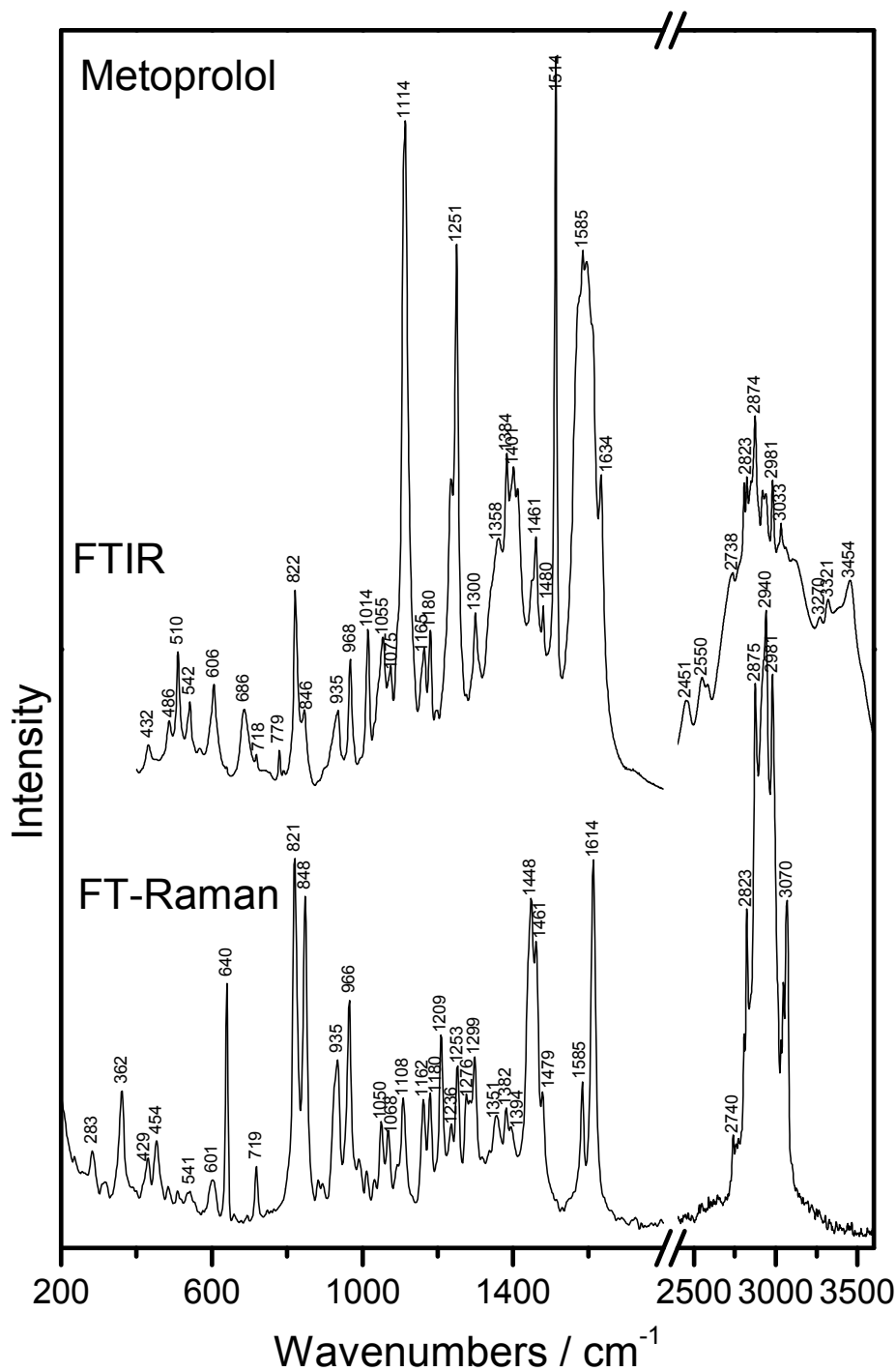


Fig. 4.2. FT-IR/ATR and FT-Raman spectra of metoprolol

The missing of the carbonyl group in this compound makes possible the clear evidence of the band corresponding to the $\delta(\text{NH}_2)$ mode at 1634 cm^{-1} in the IR spectrum. Different values are predicted for this band in the $\text{MET}^+ \cdot 2 \text{ SA}^{2-}$ complex, ranging from 1593 to 1639 cm^{-1} due to the superposition of $\nu_{\text{as}}(\text{CO}_2)$ vibrations.

The position and intensity pattern of the Q15 and Q16 mode is predicted by calculations on MET⁺ in perfect agreement with the experiment.

Two strong bands in the IR spectrum at 1251 and 1114 cm⁻¹ have as correspondents weak bands in the Raman spectrum. Their wavenumbers and their intensities are excellently reproduced by DFT calculations, both for MET⁺ and MET⁺-2 SA²⁻ structures.

Two strong bands seen in the Raman spectrum at 848 and 821 cm⁻¹ are assigned to ring breathing and to out of plane CH ring vibrations, respectively. It is worth noting here that the ring breathing vibration for MET⁺ is 38 cm⁻¹ red-shifted when compared to ATE compound.

4.3. SERS spectra of ATE and MET

Since the pKa value for the protonation of the two molecules is 9.7 and because the solution used for the SERS measurements has pH = 8.5, in order to discuss the SERS spectra we will consider the protonated forms of ATE and MET.

Raman and SERS spectra of ATE have been previously investigated by Ruperez and Laserna [39]. While their spectra are recorded in the 680–3080cm⁻¹ Raman shift range and excited with a 488 nm laser line, our spectra are recorded in the 200–3300cm⁻¹ range, being excited at 532nm.

Comparing the Raman and SERS spectra, several changes in band position and intensities can be observed, due to the interaction of ATE with the metal surface. Theoretically, the interaction of ATE with the silver surface can be established through the lone electron pairs of the oxygen and nitrogen atoms of ATE or through the π electrons of the ring.

The calculated molecular electrostatic potential (MEP) of ATE shows that the negative charge is localized mainly on the oxygen atoms and on the aromatic ring, the nitrogen atoms showing more positive charge. Thus, when added to the silver colloidal solution, the adsorption of the molecule to the silver surface is supposed to occur through the oxygen atoms. However, adsorption through the π -electrons of the aromatic ring is also plausible as predicted by the calculated MEP distribution.

Another strongly enhanced band in the SERS spectrum is observed at 1398 cm⁻¹ with a shoulder at 1423 cm⁻¹. In the Raman spectrum of unprotonated ATE the corresponding wavenumbers are 1421 and 1450 cm⁻¹, while for the protonated form, DFT calculations predict them at 1424 and 1454 cm⁻¹, respectively.

The first peak is due to COH and CH₂ deformations, while the second corresponds to CH₃ bendings in the aliphatic side chain of the ring. As seen in the SERS spectrum, these

bands are significantly red-shifted with respect to the normal Raman spectrum, suggesting the interaction of the molecule with the silver surface through the COH group.

An enhanced band is also observed at 919 cm^{-1} . For the protonated ATE, an intense Raman band is predicted at 930 cm^{-1} and another one at 899 cm^{-1} , corresponding to $\delta(\text{OH})$ and $\rho(\text{NH}_2)$ vibrations coupled with the deformation of $\text{H}_3\text{C}-\text{CH}-\text{CH}_3$ angle.

The broadening of this band is expected, as it is actually seen in the SERS spectrum, on the basis of different possible arrangements of the molecules in the vicinity of the silver surface. Therefore, it is supposed that this whole chain lies in the vicinity of the surface, the adsorption of the molecule occurring through the two O atoms of the chain.

SERS spectrum of MET shows significantly enhanced bands at 1609, 1396, 1360 and 1332 cm^{-1} . The band at 1609 cm^{-1} suggests a strong interaction of the aromatic ring with the surface, while the second is similar to that observed in the SERS spectrum of ATE at 1398 cm^{-1} , assigned to similar vibrations, i.e. deformations of the methylene and methyl groups.

The next two bands (at 1360 and 1332 cm^{-1}) cannot be seen in the SERS spectrum of ATE, being characteristic for MET molecules, both of them involving twisting of the NH_2 group.

The SERS band at 1360 cm^{-1} corresponds to the Raman band at 1351 cm^{-1} (Q20 mode) while the third one seems to be the blue-shifted Raman band at 1299 cm^{-1} (Q21 mode).

The ring breathing band at 848 cm^{-1} in the Raman spectrum appears only as a weak band in the SERS spectrum at 844 cm^{-1} , being less enhanced than the corresponding band in the SERS spectrum of ATE. Thus, according to the SERS rules [6,7] a more flat orientation of the phenyl ring relative to the silver surface is supposed for MET, compared to ATE molecules.

Moreover, as shown in Fig. 4.1., ATE is sterically hindered by the amide and the two methyl groups to lie with the aromatic ring parallel to the surface. On the other hand, the bent conformation of MET allows a more parallel alignment of the aromatic ring while the two ends of the molecule are pointing away from the silver surface.

4.4. Cu(II) complexes of ATE and MET

Molecular complexes with Cu(II) were prepared going from the starting salts (sodium benzoate and copper sulphate) by co-precipitation procedure. FT-IR spectra of the Cu(II)-ATE and Cu(II)-MET molecular complexes are given in Fig.4.3.

The strong IR band at 3356 cm^{-1} (Table 4.1), assigned to the NH_2 group of atenolol, is shifted to 3452 cm^{-1} after the complexation with copper.

Also, the very strong $\nu(\text{C}=\text{O})$ band at 1637 cm^{-1} in the IR spectrum of ATE is shifted to 1655 cm^{-1} in the spectrum of the Cu–ATE complex, showing the involvement of this oxygen atom in the coordination. The ν_{sym} band of the NH_2 group found at 3174 cm^{-1} in the spectrum of ATE shifts at a higher wavenumber (3375 cm^{-1}), suggesting the cleavage of hydrogen bonds during the complexation.

The band corresponding to the $\delta(\text{OC}-\text{NH}_2)$ vibration is redshifted from 568 cm^{-1} in the free ligand to 514 cm^{-1} in the complex. Also, a new band appears in the spectrum of the complex at 459 cm^{-1} confirming again the complexation of the Cu(II) ion by the ATE ligands, through the carbonyl group.

We note also that neither $\nu(\text{C}=\text{C})$ nor $\delta(\text{CCC})$ IR bands in the spectrum of ATE shift as a result of complexation. On the other hand, the band at 1418 cm^{-1} in the IR spectrum of the free ligand vanishes almost completely in the spectrum of the Cu–ATE complex [40].

As in the case of Cu–ATE complex, for the IR spectrum of the Cu–MET complex shown in Fig.4.3., the band characteristic for $\nu(\text{C}=\text{C})$ ring vibrations at 1512 cm^{-1} remains almost un-shifted with respect to the free ligands. The same behavior is observed for the bands at 1459 and 1178 cm^{-1} , assigned to $\delta(\text{CH}_3)$ and $d(\text{CCC ring})$, respectively.

The Q18 mode is seen at 1395 cm^{-1} (blue-shifted from 1384 cm^{-1} in the free ligand) and the band at 1299 cm^{-1} , observed for the free ligand at 1300 cm^{-1} (Q21 mode) reduces drastically in intensity. Also, the band at 1235 cm^{-1} in the spectrum of MET (mode Q23 in Table 2) is seen in the IR spectrum of the complex as a broad band with reduced intensity at 1241 cm^{-1} .

The broad bands at 1611 and 1459 cm^{-1} in the spectrum of the complex are assigned, according to Padmanabhan et al. [41], to ν_{as} and $\nu_{\text{s}}(\text{CO}_2^-)$ vibrations of the succinate anions bonded to the Cu(II) ion.

Raman spectrum of the complex (not shown here) exhibits also two bands at 236 cm^{-1} and 204 cm^{-1} which are also assigned to Cu–O vibrations with the oxygen atoms from the succinate anions.

Thus, the present data shows that Cu(II) ion is coordinated by oxygen atoms from the succinate anions. Similar coordination of Cu(II) by succinate anions was reported by Padmanabhan et al. [41] and by Vuckovic et al. [42].

Comparing the shape of the spectrum and the values of characteristic EPR parameters (A_{\parallel} , g_{\parallel} , g_{\perp}) of Cu(II)–ATE complex with those obtained for other Cu(II) complexes with nitrogen and oxygen ligands, allows us to conclude that the local symmetry around the metal ions is of square-planar type with a CuN_2O_2 chromophore in the xOy plane [43]. Such a chromophore is possible as a result of the coordination of two ATE molecules, each of them being bonded to the Cu(II) ion through the oxygen and nitrogen atoms in the amide groups [44].

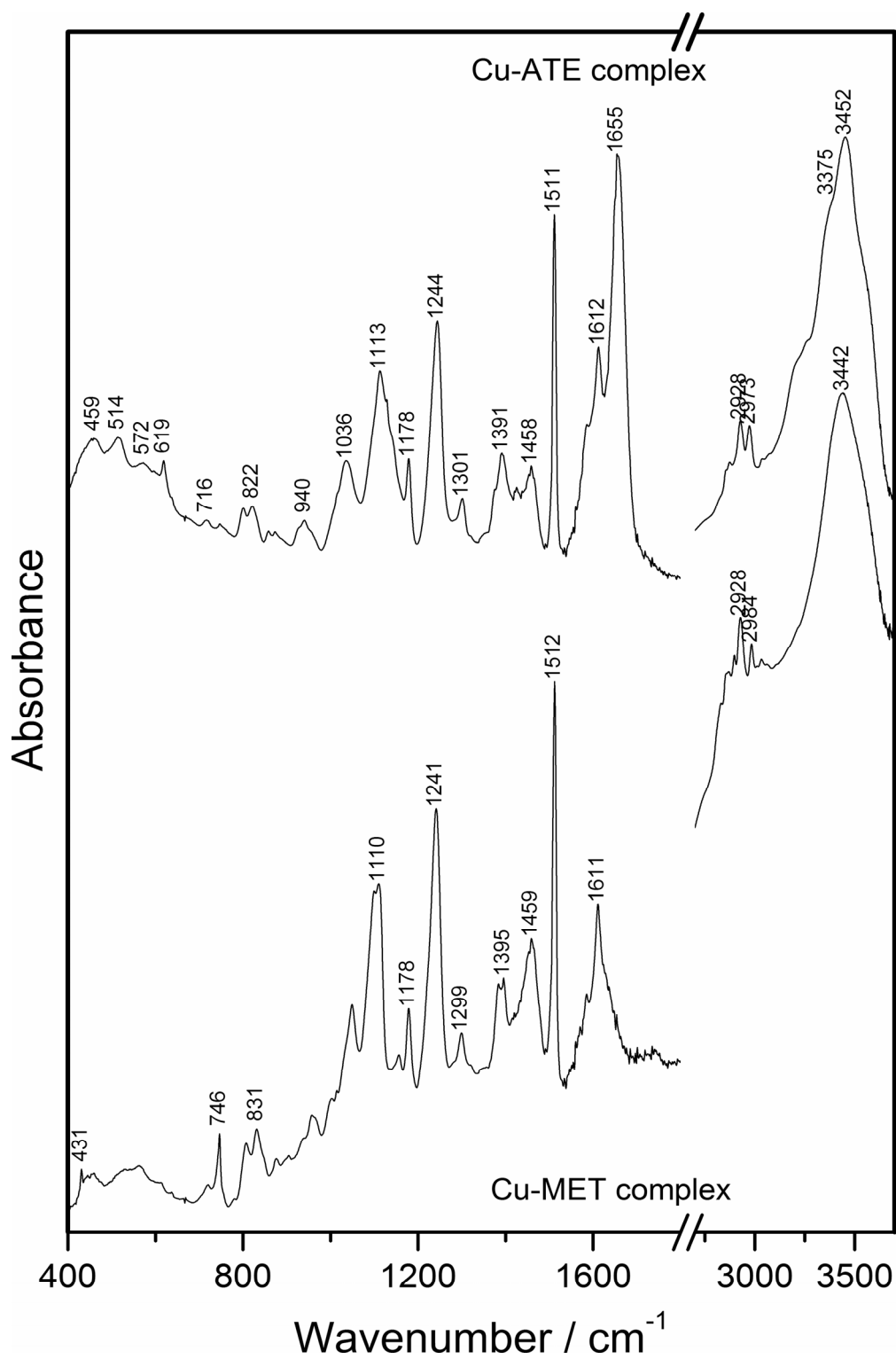


Fig. 4.3. FT-IR spectra of Cu(II)-ATE (top) and Cu(II)-MET (bottom) molecular complexes

The spectrum of Cu(II)-MET complex suggests the presence of two monomeric species, one of them with $d_{x^2-y^2}$ ground state (having $g_{\parallel} > g_{\perp}$) and the other one with d_{z^2} ground state (characterized by $g_{\perp} > g_{\parallel} = 2.0023$).

The last species is a very rare case of local symmetry which suggests the existence of strong Cu–O bonds in the case of Cu(II)–MET compound, most probably due to the coordination of the succinate anions by the Cu(II) ion.

5. Structural investigation of some metallic complexes with ligands of biomedical interest

5.1. Copper(II) complexes with ¹⁵N – labeled amino acids

The amino acid (AA) complexes with biologically active metal ions, particularly with copper (II) have received the attention because they proved to be useful antibacterial agents, nutritive supplies for humans and animals, and also as models for metalloproteins [45].

Many natural amino acids take part in the building blocks of proteins, which are chemical species indispensable to perform a large number of biological functions.

Complexes of transition metals with amino acids in proteins and peptides are utilized in numerous biological processes, such as oxygen conveyer, electron transfer and oxidation. In these processes, the enzymatic active site which is very specific, forms complexes with divalent metal ions [46].

The typically involved groups in the complexation of copper (II) by amino acids without side-chain ω-amino group are the α-amino and the carboxylate groups. The implication mode of ω-NH₂ terminal and αNH₂ / carboxylate groups in the coordination of Cu(II) L-lysine and L-ornithine complexes is reported by Conato et al. [47].

The complexation of Cu(II) with different amino acids (AA) as glycine, alanine, histidine, serine, proline, tyrosine, phenylalanine, glutamine, glutamic acid, cysteine, leucine, arginine etc. was the investigated subject of many papers [6-9]. The general coordination type for Cu(II) with two α – amino acids is the binding of both AA by an amino nitrogen and a carboxyl oxygen, i.e. a NNOO coordination or a glycine – like bonding.

Labelled stable isotopes (¹⁵N-Lysine, ¹⁵N-Ornithine) are used in a variety of studies, offering the ideal internal standards in quantitative information in isotopic tracers for nutrition investigations, to elucidate details of nitrogen metabolism in vivo and protein metabolism in different diseases [48]. All these studies demands accurate measurements of the isotopic abundances of each tracer by mass spectrometry coupled with chromatography and NMR in conjunction with tracer methodologies.

A comparative IR study between D,L-Lysine and D,L-Ornithine amino acids and their [¹⁵N]-labeled forms is presented in continuation. The behaviour of their copper (II) complexes on NaY and HY type zeolites is also investigated by ESR spectroscopy [49].

5.2. The identification of some monomeric species in the case of adsorption on NaY and HY zeolites

The Cu²⁺ ion is surrounded by two N and two O atoms from the α -amino and carboxylate groups in a square planar coordination by ligation of two lysine or ornithine molecules.

In the case of aqueous solutions, the characteristic spectra of the investigated compounds show well resolved hyperfine copper lines ($I_{Cu} = 3/2$) typical for high rate of tumbling motion.

The ¹⁵N-superhyperfine lines ($I=1/2$) due to the interaction of paramagnetic electron with two equivalent nitrogen nuclei appear clearly on the high field copper hyperfine peak (+3/2) of lysine compound. The isotropic nitrogen hyperfine splitting is of 18G ($17.8 \times 10^{-4} \text{ cm}^{-1}$) and the g_0 and A_0 values are 2.122; 2.126 and 67.5; 68.4G for both compounds, respectively.

ESR spectra of these compounds adsorbed on NaY and HY zeolites are shown in Fig. 5.1.

The immobilized monomeric species of Cu(AA)₂²⁺ compounds in the supercages (III type sites) of the NaY zeolite (Fig. 5.1b) which has cavity diameters $\sim 13 \text{ \AA}$ and an water content of 26.4%, have a tetragonal elongated octahedral symmetry due to the coordination of two water molecules at Cu²⁺ ion along the Oz axis (apical positions).

In the case of HY zeolite with 13% water content and smaller cavity diameters ($\sim 8 \text{ \AA}$), two different magnetically nonequivalent monomeric species were evidenced (Fig. 5.1a).

The first species having the following ESR parameters $g_{\parallel} = 2.251$, $A_{\parallel} = 173.7 \times 10^{-4} \text{ cm}^{-1}$ for Cu(II) - ¹⁵N – Lysine compound and $g_{\parallel} = 2.251$, $A_{\parallel} = 177.9 \times 10^{-4} \text{ cm}^{-1}$ for Cu(II) - ¹⁵N – Ornithine may be considered also immobilized in the III type sites of supercages. Their local symmetry is of tetragonal – octahedral (Oh) distorted type analogue with that from NaY zeolite. However in this case the two water molecules coordinated at Cu²⁺ ion along the Oz axis are stronger bound than in the case of NaY zeolite, leading to a real axial perturbation and to the hexacoordinated form of the metallic ion.

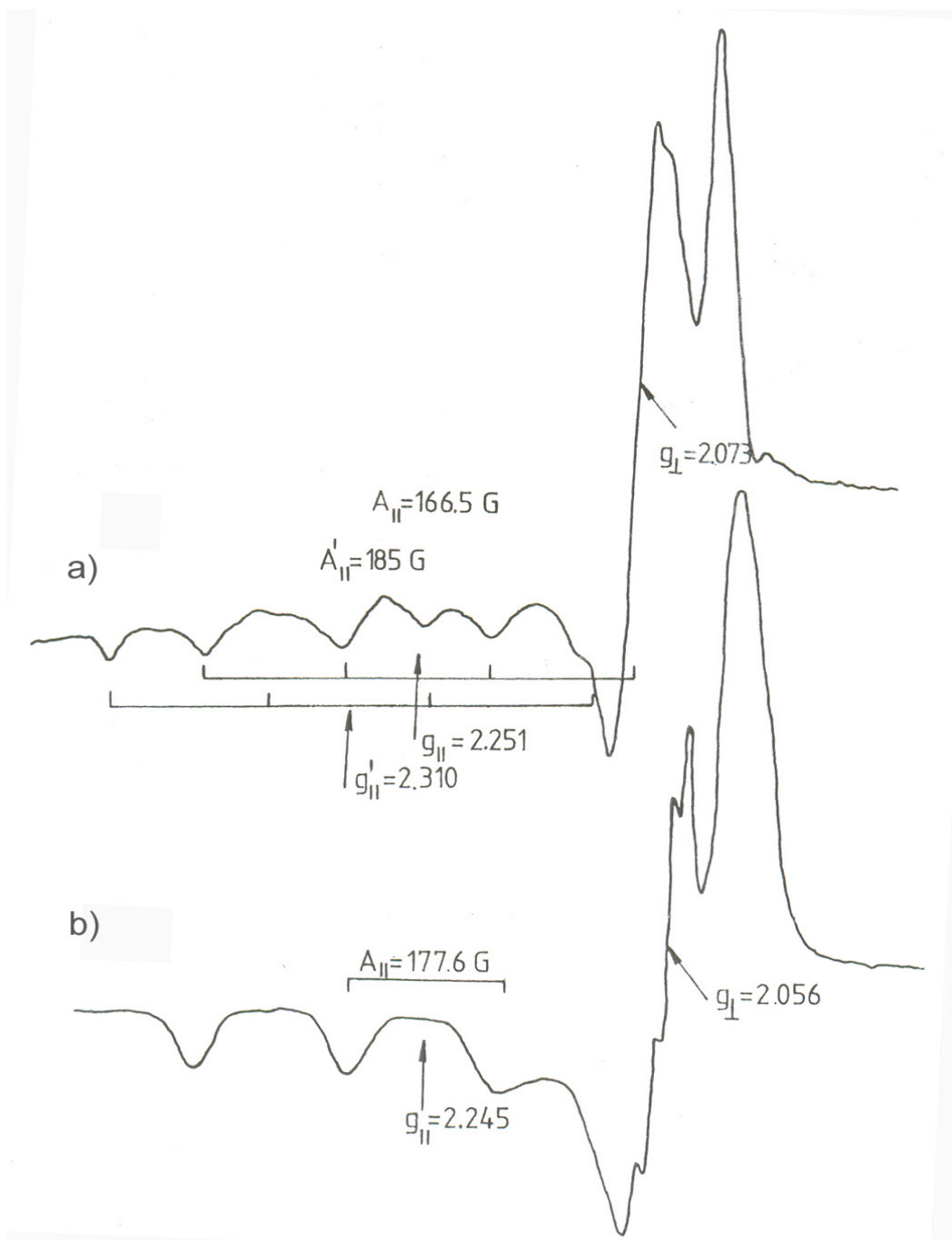


Fig. 5.1. Room temperature ESR spectra of Cu(II) – ^{15}N – Lysine compound adsorbed on HY (a) and NaY (b) zeolites

The second species from HY zeolite are located on the walls of the cavities, in the S_{II} sites, and their $\text{OH}(\text{OH}_2)$ groups are stronger coordinated to Cu^{2+} ion than other water molecules from inner of the cavities, resulting in a slight distorted C_{4v} (square-pyramidal) local symmetry.

ESR characteristic parameters for all monomeric species of Cu(II) – ^{15}N -Lysine compound adsorbed on NaY and HY zeolites are given in Table 5.1.

Table 5.1. ESR parameters of Cu(II) – ¹⁵N – Lysine complex at room temperature*

Nr. crt.	Sample	g	g _⊥	A	A _⊥	α ²	β ²	G	f
1	powder	2.252	2.063	202.3	22.5	0.839	0.626	4.10	109.70
		2.217	2.054					4.13	
2	absorbed on NaY zeolite	2.245	2.056	184.7	19	0.819	0.725	4.50	121.54
3	absorbed on HY zeolite	2.251	2.060	173.7		0.795	0.765	4.29	129.59
		2.310	2.073	198.7				4.33	116.25
4	absorbed on HY zeolite after suppl. dehydr.	2.373	2.075	139	19.2	0.828	0.845*	5.09	170.71

* - hyperfine parameters are given in 10⁻⁴ cm⁻¹

The ESR parameter values (g_{||} = 2.373, A_{||} = 139 x 10⁻⁴ cm⁻¹) characteristic for monomeric species which appears in HY zeolite after a supplementary dehydration at 80⁰C suggests a tetrahedral (Td) symmetry around Cu²⁺ ions. In this case one or both lysine molecules are replaced by OH, H₂O groups of the support surface.

5.3. IR and NMR results on Pd(II) complex with theophylline and bipyridine

Several research groups investigated the coordination of metal ions to biologically important purine derivatives – adenine and guanine, which are major constituents of DNA and RNA – and xanthine and hypoxanthine, which are minor constituents of RNA [50].

The metal complexes of N-methyl substituted xanthines – theophylline (Fig. 5.2), theobromine and caffeine – are also of major interest, because these ligands can serve as models for biologically important analogues. Due to its similarity to guanine, theophylline has been studied most intensively.

The two ν(C=O) stretching vibrations (1695 cm⁻¹; 1637 cm⁻¹) from the IR spectrum of the complex are recorded at smaller wavenumbers than in the free theophylline IR spectrum (1717 cm⁻¹, 1669 cm⁻¹). These shifts (Table 5.2) are mainly due to the deprotonation at the N(7) atom of theophylline and coordination through this atom to the metal centre [51].

The ν(C=N) vibrations are also shifted at lower wavenumbers due to the coordination through N(7) atom in the case of theophylline, and N(2) and N(2') atoms in the case of 2,2'-bipyridine. In N(7)-bonded theophyllinato complexes, the carbonyl group is generally hydrogen-bonded with other ligands in the metal coordination sphere.

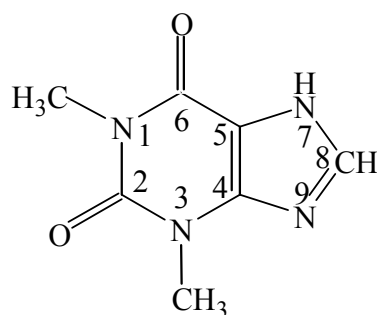


Fig.5.2. The structure of theophylline

The $^1\text{H-NMR}$ spectrum of theophylline shows four singlets at 13.57, 8.04, 3.44, 3.23 ppm which are assigned to N(7)H, C(8)H and to the two methyl group protons, respectively.

The absence of the HN(7) resonance from the $^1\text{H-NMR}$ spectrum of the complex demonstrates that theophylline coordinates in the deprotonated form. The shifted of theophylline HC(8) resonance to smaller values with 0.36 ppm in the $[\text{Pd}(\text{th})_2(2,2'\text{-bipy})]\cdot\text{H}_2\text{O}$ complex is another evidence of the coordination of theophylline through the adjacent N(7) atom.

Table 5.2. Vibrational bands assignment for ligands and $[\text{Pd}(\text{th})_2(2,2'\text{-bipy})]\cdot\text{H}_2\text{O}$ compound [cm^{-1}]

Compound	$\nu(\text{OH})$	$\nu(\text{NH})$	$\nu(\text{CH})$	$\nu(\text{C}=\text{O})$	$\nu(\text{C}=\text{N})$
Theophylline	3348 w	3122 m	2985 m	1717 s	1568 s
$(\text{C}_7\text{H}_8\text{N}_4\text{O}_2)$			2825 m	1669 vs	
2,2'-Bipyridine			3151-3000 m		1577 vs
$(\text{C}_{10}\text{H}_8\text{N}_2)$			2925 m		1560 s
$[\text{Pd}(\text{th})_2(2,2'\text{-bipy})]\cdot\text{H}_2\text{O}$	3463 w		3118-3050 w	1695 vs	1529 s
			2949 w	1637 vs	

The $^1\text{H-NMR}$ spectrum of 2,2'-bipyridine shows four signals at 8.71, 8.41, 7.84 and 7.33 ppm, respectively, which are assigned to HC(5), HC(2), HC(3), HC(4) protons. Due to coordination, the resonances of HC(5) and HC(2) protons are shifted to smaller values, and the resonances of HC(3) and HC(4) are shifted to bigger values of chemical shifts.

5.4. Structural informations obtained by X-ray diffraction and DFT calculations

Crystal structure of $[\text{Pd}(\text{th})_2(2,2'\text{-bipy})]\cdot\text{H}_2\text{O}\cdot(\text{C}_6\text{H}_{14})$ determined by X-ray diffraction shows that the palladium atom is bonded to two theophylline ligands through the deprotonated N(7) atoms and to the 2,2'-bipyridine molecule through N(2) and N(2') atoms. The coordination polyhedron of the metal atom adopts a distorted square-planar geometry.

The bipyridine ligands are stacked along the c axis (Fig. 5.3.); the distance between the center of two benzol rings of the partially overlapped bipyridine fragments is 3.56 Å, which is the normal range for $\pi \cdots \pi$ stacking interactions [52].

DFT structure optimization of $[\text{Pd}(\text{th})_2(2,2'\text{-bipy})]$ was performed with the Gaussian '98 program, starting from a pre-optimized X-ray geometry in PC Spartan Pro. The calculations employed the B3LYP exchange functional using LANL2DZ basis set. The Molekel view of the optimized structure of $[\text{Pd}(\text{th})_2(2,2'\text{-bipy})]$ is shown in Fig. 5.4 [15].

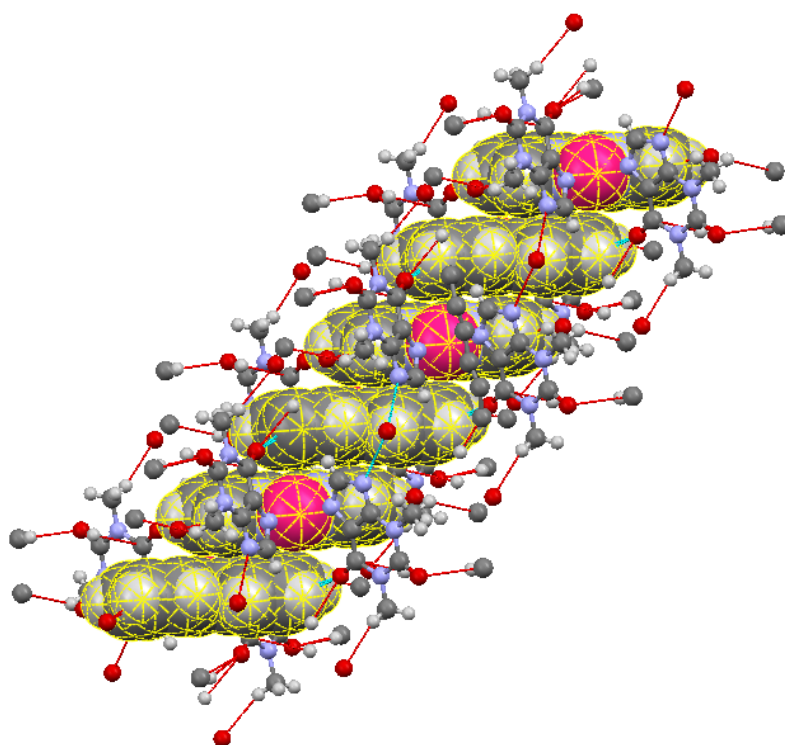


Fig. 5.3. The packing in the crystal of $[\text{Pd}(\text{th})_2(2,2'\text{-bipy})] \cdot \text{H}_2\text{O} \cdot (\text{C}_6\text{H}_{12})$ emphasizing the $\pi \cdots \pi$ stacking through the bipyridine rings

In the optimized structure the square coordination is almost planar. Furthermore, the atoms of the 2,2'-bipyridine rings are almost coplanar and the purine molecules are also practically planar. In the solid state structure, the 2,2'-bipyridine rings are twisted around the 1,1'-carbon bond, the N2-C1-C1'-N2' dihedral angle being -7.5° , which is 3.3° greater than that of the average of palladium complexes containing a Pd(bipy) unit. These deviations from planarity can be attributed to packing effects.

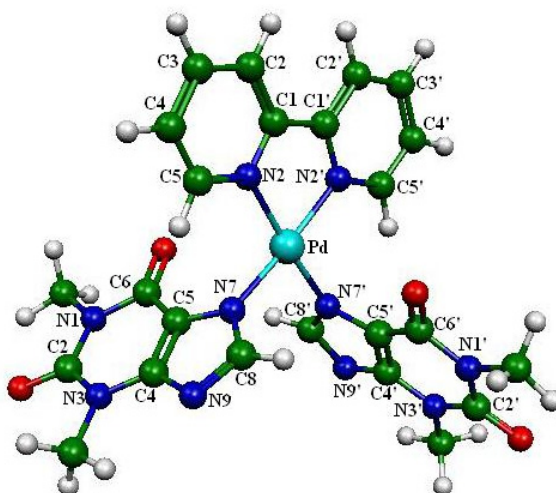


Fig. 5.4. Molekel view of the optimized structure of [Pd(th)₂(2,2'-bipy)] complex

CONCLUSIONS

The very good correlations between recorded FT-IR, FT-Raman and SERS spectra of paroxetine with those obtained by DFT calculations certify a very good optimization of the molecular geometry.

Based on the analysis of SERS and Raman spectra and considering the MEP map of this molecule and the SERS selection rules, the adsorption mode of paroxetine to silver nanoparticles was shown to occur through the oxygen (O1, O3, O10) and nitrogen (N22) atoms.

The benzodioxol ring is adsorbed in a tilted orientation, in the near vicinity of the silver surface, while the piperidine ring and benzene ring are perpendicular oriented on the silver surface.

The adsorption mode of pindolol (PIN) and verapamil (VER) molecules on the silver nanoparticles surface was also established following the same procedure.

Based on the MEP maps which show the most electronegative sites of these molecules and SERS selection rules, the adsorption of PIN and VER on silver nanoparticles was shown to occur preponderantly through the oxygen atoms and the ring π -electrons.

The interaction of the oxygen atoms and silver surface is illustrated by the presence of the SERS bands at 238–240 cm^{-1} due to the occurrence of Ag-O bonds, for both investigated molecules.

The two molecules PIN and VER are adsorbed to the silver surface in a flat and bent orientation, respectively.

A detailed description of vibrational IR and Raman spectra of atenolol (ATE) and metoprolol (MET) compounds is given at B3LYP/6-31G(d) level of theory, performed on S and RS conformers for ATE and protonated form MET⁺ and MET⁺ - 2 succinate anions (SA²⁻) compound.

Based on the analysis of the SERS spectra and the corresponding selection rules, the adsorption of ATE and MET on silver nanoparticles was shown to occur through the oxygen atoms and the ring π -electrons, with the phenyl ring in the close vicinity of the silver surface.

The coordination mode of the metal ions in Cu(II)-ATE and Cu(II)-MET molecular complexes was also derived from IR, Raman and ESR spectra. A square-planar arrangement with N₂O₂ chromophore around the copper (II) ion is realized in the case of ATE compound, while only oxygen atoms are involved in the coordination of Cu-MET complex.

ESR spectra of Cu(II)-[¹⁵N]-Lysine (Ornithine) complexes adsorbed on NaY and HY zeolites allowed us to establish the local symmetry of four monomeric species which appear in their supercages.

The empirical factor of tetragonal distortion (f) has the values in the 109-120 range showing that these monomeric species have in principle a slightly distorted square-planar arrangement.

For all these species, the in-plane σ bond has an ionic character ($\alpha^2 \cong 0.80$) while the in-plane π bond is more covalent ($\beta^2 \cong 0.73$) than that of the σ type.

We have established from IR and NMR spectra of the ligand molecules and [Pd(th)₂(2,2'- bipy)]·H₂O compound that theophylline coordinates at metal ion in a deprotonated form by N7 atom and 2,2' - bipyridine by N2, N2' atoms.

Single crystal X-ray diffraction analysis and DFT calculations demonstrated that the [Pd(th)₂(2,2'- bipy)]·H₂O·(C₆H₁₄) has a distorted square planar coordination around the Pd(II). The deviation from planarity is a consequence of packing effects.

References

1. S. Aștilean, Metode și tehnici moderne de spectroscopie optică, vol.I, Spectroscopia IR și Raman, Ed. Casa Cărții de Știință, Cluj-Napoca, 2002
2. T.Iliescu, S.Cântă-Pânzaru, D.Maniu, R.Grecu, S.Aștilean, Aplicații ale Spectroscopiei vibraționale, Ed.Casa Cărții de Știință, Cluj-Napoca, 2002
3. L. David, O. Cozar, C. Cristea, L. Gaina, Identificarea structurii moleculare prin metode spectroscopice, Ed. Presa Universitară Clujeană, 2002
4. N.Leopold, J.R. Baena, M.Bolboacă, O.Cozar, W.Kiefer, B.Lendl, *Vibr. Spectroscopy*, 36, 47(2004)
5. N.B.Colthup, L.H.Daly, S.E.Wilberley, Introduction to Infrared and Raman Spectroscopy, Acad.Press, San Diego, 1990
6. M. Baia, S. Aștilean, T. Iliescu, Raman and SERS Investigations of Pharmaceuticals, Ed. Springer-Verlag, Berlin, Heidelberg, 2008
7. T. Iliescu, S. Pînzaru, Spectroscopia Raman și SERS cu aplicații în biologie și medicină, Ed. Casa cărții de știință, Cluj-Napoca, 2011
8. N. Leopold, Surface Enhanced Raman Spectroscopy – Selected Applications, Ed. Napoca Star, 2009
9. N. Leopold, B. Lendl, *J. Phys. Chem.*, B107, 5723(2003)
10. L. Szabo, V. Chiș, A. Pîrnău, N. Leopold, O. Cozar, *Sz. Orosz, J. Molec. Struct.*, 924-926, 385(2009)
11. C.P. Slichter, Principles of Magnetic Resonance, Third enlarged and updated edition, Ed. Springer – Verlag Berlin, Heidelberg, New York, 1996
12. R. Fechete, D.E. Demco, D.C. Moldovan, R.I. Chelcea, E. Culea, Rezonanța Magnetică Nucleară – Metode clasice și moderne, Ed. Risoprint, Cluj-Napoca, 2010
13. V. Chiș, A. Pîrnău, T. Jurca, M. Vasilescu, S. Simon, O. Cozar, L. David, *Chem. Phys.*, 316, 153(2005)
14. A.Pîrnău, Corelări teoretice-experimentale în analiza unor compuși de interes biomedical, Ed.Presa Univ.Clujeană, 2007
15. P. Flukiger, H.P. Luhti, S. Portmann, J. Weber, MOLEKEL 4.2, Swiss Center for Scientific Computing, Manno (Switzerland), 2000–2002
16. N. Leopold, V. Chiș, *I.B. Cozar*, L. Szabo, A. Pîrnău, O.Cozar, *Opt. Adv. Mater. Rapid Commun.*, 2, 278(2008)
17. T. Hestekamp, J. Barker, A. Davenport, M. Whittaker, *Curr. Top. Med. Chem.*, 7, 1582(2007)

18. N. Beckmann, R. Kneuer, H.U. Gremlich, H. Karmouty-Quintana, F.X. Blé, M. Müller, *NMR Biomed*, 20, 154(2007)
19. S.J. Mathew, R.B. Price, D.C. Shungu, X. Mao, E.L.P. Smith, J.M. Amiel, J.D. Coplan, *J. Psychopharmacol*, 24, 1175(2010)
20. M. Urbanova, V. Setnicka, P. Bour, H. Navratilova, K. Volka, *Biopolymers*, 67(4– 5), 298(2002)
21. M.R. Caira, E. de Vries, L.R. Nassimbeni, V.W. Jacewicz, *J. Incl. Phenom. Macro. Chem.*, 46, 37(2003)
22. *I.B. Cozar*, L. Szabo, D. Mare, N. Leopold, L. David, V. Chiş, *J. Molec. Struct.*, 993, 243(2011)
23. S. Mishra, R.K. Singh, A.K. Ojha, *Chem. Phys.*, 355, 14(2009)
24. P.S. Mdluli, N.M. Sosibo, N. Revrapasadu, P. Karamanis, J. Leszczynski, *J. Mol. Struct.*, 935, 32(2009)
25. J. Ballesteros, L.F. Callado, *J. Affect. Disord.*, 79, 137(2004)
26. E. Beck, W.J. Sieber, R. Trejo, *Am. Fam. Phys.*, 71, 717(2005)
27. R.A.E. Castro, J. Canotilho, S.C.C. Nunes, M.E.S. Eusébio, J.S. Redinha, *Spectrochim. Acta A*; 72, 819(2009)
28. S.C.C. Nunes, M.E. Eusébio, M.L.P. Leitão, J.S. Redinha, *Int. J. Pharm.*, 285, 13(2004)
29. B. Fernandez, R. Mosquera, E. Uriarte, *Inter. J. Pharm.*, 79, 199(1992)
30. *I.B. Cozar*, L. Szabo, N. Leopold, V. Chiş, O. Cozar, L. David, *J. Molec. Structure*, 993, 308(2011)
31. T.K. Chattopadhyay, R.A. Palmer, D. Mahadevan, *J. Chem. Crystallogr.*, 25, 195(1995)
32. D.S. Wishart, C. Knox, A.C. Guo, D. Cheng, S. Shrivastava, D. Tzur, B. Gautam, M. Hassanali, *Nucl. Acids Res.*, 36(2008) ((Database Issue):D901-6. PMID:18048412)
33. S.C.C. Nunes, A.J. Lopes Jesus, M.T.S. Rosado, M.E.S. Eusébio, *J. Mol. Struct. (Theochem)*, 806, 231(2007)
34. A.P. Scott, L. Radom, *J. Phys. Chem.* 100, 16502(1996)
35. *I.B. Cozar*, L. Szabo, O. Cozar, N. Leopold, V. Chiş, L. David, IR, SERS and DFT Study of Pindolol and Verapamil Drugs, 30th European Congress on Molecular Spectroscopy, Florence(I), 29Aug. – 3 Sept. 2010, p.100
36. R.A. E. Castro, J. Canotilho, R.M. Barbosa, J.S. Redinha, *Spectrochim. Acta A*, 67, 1194(2007)

37. *I.B. Cozar*, L. Szabo, N. Leopold, V. Chiş, L. David, *Rom. J. Phys.*, 55, 772(2010)
38. G. Bartolucci, B. Bruni, S.A. Coran, M. Di Vaira, *Acta Cryst.*, E65, o1364(2009)
39. Ruperez, J.J. Laserna, *Anal. Chim. Acta*, 335, 87(1996)
40. O. Cozar, L. Szabo, *I.B. Cozar*, N. Leopold, L. David, C. Căinap, V. Chiş, *J. Molec. Struct.*, 993, 357(2011)
41. M. Padmanabhan, S.M. Kumary, X.Huang, J. Li, *Inorg. Chim. Acta*, 358, 3537(2005)
42. G. Vuckovic, M. Antonijevic-Nikolicb, T. Lis, J. Mrozinski, M. Korabik, D.D. Radanovic, *J. Molec. Struct.*, 872, 135(2008)
43. E. Manoj, M.R.P. Kurup, A. Punnoose, *Spectrochim. Acta A*, 72, 474(2009)
44. Z. Wang, D.R. Powell, R.P. Houser, *Inorg. Chim. Comm.*, 12, 511(2009)
45. M.Z. Iqbal, S. Kurshid, M.S. Iqbal, J. Pak, *Med. Assoc.*, 40, 221(1990)
46. T.Vemrlinov, S.Arpadjan, I.Karadjova, J.Beattie, *Acta Pharm.*, 56, 105(2006)
47. C.Conato, A.Contino, G.Maccarrone, A.Magri, M.Remelli, G.Tabbi, *Thermochimica Acta*, 362, 13(2000)
48. D.Mavri-Damelin, S.Eaton, L.H.Damelin, M.Rees, H.J.Hodgson, C.Selden, *Int.J.Biochem. Cell Biol.*, 39, 555(2007)
49. O. Cozar, I. Bratu, L. Szabo, *I.B. Cozar*, V. Chiş, L. David, *J. Molec.Struct.*, 993, 397(2011)
50. T. J. Kistenmacher, D. J. Szalda, L. G. Marzilli, *Inorg. Chem.*, 14, 1686(1975)
51. E. Forizs, A. Debreczeni, A. Patrut, A.Z. Kun, *I.B. Cozar*, L. David, I. Silaghi-Dumitrescu, *Rev. Roum. de Chimie*, 55(10), 697(2010)
52. H.C. Freeman, M. R. Snow, *Acta Cryst.*, 18, 843(1965)

Acknowledgements

I wish to express the most sincere thanks to Prof. Dr. Leontin David for his competent guidance and assistance provided during the thesis development.

I thank also very much to Prof. Dr. Vasile Chiş for his support and relevant suggestions in DFT calculations, experimental results interpretation and scientific papers completion.

Sincere thanks to Assoc. Prof. Dr. Nicolae Leopold for his assistance in performing experimental measurements (especially SERS), obtaining and interpretation of experimental results and for all his competent advice.

I thank to Physicist Dr. Laszlo Szabo for help and fruitful cooperation experienced during these years.

I would like to thank also to Prof. Dr. Edit Forizs from the Faculty of Chemistry and Chemical Engineering and to Scientific Researcher Dr. Ioan Bratu from INCDTIM Cluj-Napoca for their cooperation in the thesis development.

I express my deepest gratitude to my parents for all their constant support.